3. Mitsuya H, Maeda K, Das D, Ghosh AK. 2008. Development of protease inhibitors and the fight with drug-resistant HIV-1 variants. Adv. Pharmacol. 56:169–197.
4. Walensky RP, Paltiel AD, Losina E, Mercincavage LM, Schackman BR, Sax PE, Weinstein MC, Freedberg KA. 2006. The survival benefits of AIDS treatment in the United States. J. Infect. Dis. 194:11–19.
5. De Clercq E. 2002. Strategies in the design of antiviral drugs. Nat. Rev. Drug Discov. 1:13–25.
6. Siliciano JD, Siliciano RF. 2004. A long-term latent reservoir for HIV-1. J. Antimicrob. Chemother. 54:6–9.
7. Simon V, Ho DD. 2003. HIV-1 dynamics in vivo: implications for therapy. Nat. Rev. Microbiol. 1:181–190.
8. Carr A. 2003. Toxicity of antiretroviral therapy and implications for drug development. Nat. Rev. Drug Discov. 2:624–634.
9. Fumero E, Podzamczer D. 2003. New patterns of HIV-1 resistance during HAART. Clin. Microbiol. Infect. 9:1077–1084.
10. Grabar S, Weiss L, Costagliola D. 2006. HIV infection in older patients in the HAART era. J. Antimicrob. Chemother. 57:4–7.
11. Hirsch HH, Kaufmann G, Sendi P, Battegay M. 2004. Immune reconstitution in HIV-infected patients. Clin. Infect. Dis. 38:1159–1166.
12. Little SJ, Holte S, Routy JP, Daar ES, Markowitz M, Collier AC, Koup RA, Mellors JW, Connick E, Conway B, Kilby M, Wang L, Whitcomb JM, Hellmann NS, Richman DD. 2002. Antiretroviral-drug resistance among patients recently infected with HIV. N. Engl. J. Med. 347:385–394.
13. Naggie S, Hicks C. 2010. Protease inhibitor-based antiretroviral therapy in treatment-naive HIV-1-infected patients: the evidence behind the options. J. Antimicrob. Chemother. 65:1094–1099.
14. Ghosh AK, Kincaid JF, Cho W, Walters DE, Krishnan K, Hussain KA, Koo Y, Cho H, Rudall C, Holland L, Buthod J. 1998. Potent HIV protease inhibitors incorporating high-affinity P2-ligands and (R)-(hydroxyethylamino)sulfonamide isostere. Bioorg. Med. Chem. Lett. 8:687–690.
15. Ghosh AK, Krishnan K, Walters DE, Cho W, Cho H, Koo Y, Trevino J, Holland L, Buthod J. 1998. Structure based design: novel spirocyclic ethers as nonpeptidal P2-ligands for HIV protease inhibitors. Bioorg. Med. Chem. Lett. 8:979–982.
16. Koh Y, Nakata H, Maeda K, Ogata H, Bilcer G, Devasamudram T, Kincaid JF, Boross P, Wang YF, Tie Y, Volarath P, Gaddis L, Harrison RW, Weber IT, Ghosh AK, Mitsuya H. 2003. Novel bis-tetrahydrofuranylurethane-containing nonpeptidic protease inhibitor (PI) UIC-94017 (TMC114) with potent activity against multi-PI-resistant human immunodeficiency virus in vitro. Antimicrob. Agents Chemother. 47:3123–3129.
17. Ghosh AK, Xu CX, Rao KV, Baldridge A, Agniswamy J, Wang YF, Weber IT, Aoki M, Miguel SG, Amano M, Mitsuya H. 2010. Probing multidrug-resistance and protein-ligand interactions with oxatricyclic designed ligands in HIV-1 protease inhibitors. ChemMedChem 5:1850–1854.
18. Shirasaka T, Kavlick MF, Ueno T, Gao WY, Kojima E, Alcaide ML, Chokekijchai S, Roy BM, Arnold E, Yarchoan R, Mitsuya H. 1995. Emergence of human immunodeficiency virus type 1 variants with resistance to multiple dideoxynucleosides in patients receiving therapy with dideoxynucleosides. Proc. Natl. Acad. Sci. U. S. A. 92:2398–2402.
19. Yoshimura K, Kato R, Kavlick MF, Nguyen A, Maroun V, Maeda K, Hussain KA, Ghosh AK, Gulnik SV, Erickson JW, Mitsuya H. 2002. A potent human immunodeficiency virus type 1 protease inhibitor, UIC-94003 (TMC-126), and selection of a novel (A28S) mutation in the protease active site. J. Virol. 76:1349–1358.
20. Yoshimura K, Kato R, Yusa K, Kavlick MF, Maroun V, Nguyen A, Mimoto T, Ueno T, Shintani M, Falloon J, Masur H, Hayashi H, Erickson J, Mitsuya H. 1999. JE-2147: a dipeptide protease inhibitor (PI) that potently inhibits multi-PI-resistant HIV-1. Proc. Natl. Acad. Sci. U. S. A. 96:8675–8680.
21. Ghosh AK, Leshchenko S, Noetzel M. 2004. Stereoselective photochemical 1,3-dioxolane addition to 5-alkoxymethyl-2(5H)-furanone: synthesis of bis-tetrahydrofuranyl ligand for HIV protease inhibitor UIC-94017 (TMC-114). J. Org. Chem. 69:7822–7829.
22. Maeda K, Yoshimura K, Shibayama S, Habashita H, Tada H, Sagawa K, Miyakawa T, Aoki M, Fukushima D, Mitsuya H. 2001. Novel low molecular weight spirodiketopiperazine derivatives potently inhibit R5 HIV-1 infection through their antagonistic effects on CCR5. J. Biol. Chem. 276:35194–35200.
23. Nakata H, Amano M, Koh Y, Kodama E, Yang G, Bailey CM, Kohgo S, Hayakawa H, Matsuoka M, Anderson KS, Cheng YC, Mitsuya H. 2007. Activity against human immunodeficiency virus type 1, intracellular metabolism, and effects on human DNA polymerases of 4′-ethynyl-2-fluoro-2′-deoxyadenosine. Antimicrob. Agents Chemother. 51:2701–2708.
24. Amano M, Koh Y, Das D, Li J, Leschenko S, Wang YF, Boross PI, Weber IT, Ghosh AK, Mitsuya H. 2007. A novel bis-tetrahydrofuranylurethane-containing nonpeptidic protease inhibitor (PI), GRL-98065, is potent against multiple-PI-resistant human immunodeficiency virus in vitro. Antimicrob. Agents Chemother. 51:2143–2155.
25. Ide K, Aoki M, Amano M, Koh Y, Yedidi RS, Das D, Leschenko S, Chapsal B, Ghosh AK, Mitsuya H. 2011. Novel HIV-1 protease inhibitors (PIs) containing a bicyclic P2 functional moiety, tetrahydropyranotetrahydrofuran, that are potent against multi-PI-resistant HIV-1 variants. Antimicrob. Agents Chemother. 55:1717–1727.
26. Tojo Y, Koh Y, Amano M, Aoki M, Das D, Kulkarni S, Anderson DD, Ghosh AK, Mitsuya H. 2010. Novel protease inhibitors (PIs) containing macrocyclic components and 3(R),3a(S),6a(R)-bis-tetrahydrofuranylurethane that are potent against multi-PI-resistant HIV-1 variants in vitro. Antimicrob. Agents Chemother. 54:3460–3470.
27. Kaminski GA, Friesner EA. 2001. Evaluation and reparametrization of the OPLS-AA force field for proteins via comparison with accurate quantum chemical calculations on peptides. J. Phys. Chem. B 105:6474–6487.
28. Koh Y, Amano M, Towata T, Danish M, Leshchenko-Yashchuk S, Das D, Nakayama M, Tojo Y, Ghosh AK, Mitsuya H. 2010. In vitro selection of highly darunavir-resistant and replication-competent HIV-1 variants by using a mixture of clinical HIV-1 isolates resistant to multiple conventional protease inhibitors. J. Virol. 84:11961–11969.
29. Schon A, Ingaramo M, Freire E. 2003. The binding of HIV-1 protease inhibitors to human serum proteins. Biophys. Chem. 105:221–230.
30. Marcelin AG, Affolabi D, Lamotte C, Mohand HA, Delaugerre C, Wirden M, Voujon D, Bossi P, Ktorza N, Bricaire F, Costagliola D, Katlama C, Peytavin G, Calvez V. 2004. Resistance profiles observed in virological failures after 24 weeks of amprenavir/ritonavir containing regimen in protease inhibitor experienced patients. J. Med. Virol. 74:16–20.
31. Young TP, Parkin NT, Stawiski E, Pilot-Matias T, Trinh R, Kempf DJ, Norton M. 2010. Prevalence, mutation patterns, and effects on protease inhibitor susceptibility of the L76V mutation in HIV-1 protease. Antimicrob. Agents Chemother. 54:4903–4906.
32. Aoki M, Danish ML, Aoki-Ogata H, Amano M, Ide K, Koh Y, Mitsuya H. 2012. The loss of protease dimerization inhibition activity of tipranavir (TPV) and its association with HIV-1 acquisition of resistance to TPV. J. Virol. 86:13384–13396.
33. Wlodawer A, Vondrasek J. 1998. Inhibitors of HIV-1 protease: a major success of structure-assisted drug design. Annu. Rev. Biophys. Biomol. Struct. 27:249–284.
34. Wlodawer A, Erickson JW. 1993. Structure-based inhibitors of HIV-1 protease. Annu. Rev. Biochem. 62:543–585.
35. Koh Y, Matsumi S, Das D, Amano M, Davis DA, Li J, Leschenko S, Baldridge A, Shioda T, Yarchoan R, Ghosh AK, Mitsuya H. 2007. Potent inhibition of HIV-1 replication by novel non-peptidyl small molecule inhibitors of protease dimerization. J. Biol. Chem. 282:28709–28720.
36. Dunn BM, Goodenow MM, Gustchina A, Wlodawer A. 2002. Retroviral proteases. Genome Biol. 3:reviews3006.1-reviews3006.7. doi:10.1186/gb-2002-3-4-reviews3006.
37. Fournier T, Medjoubi NN, Porquet D. 2000. Alpha-1-acid glycoprotein. Biochim. Biophys. Acta 1482:157–171.
38. Boffito M, Miralles D, Hill A. 2008. Pharmacokinetics, efficacy, and safety of darunavir/ritonavir 800/100 mg once-daily in treatment-naïve and -experienced patients. HIV Clin. Trials 9:418–427.

THE JOURNAL OF BIOLOGICAL CHEMISTRY VOL. 288, NO. 22, pp. 15813–15820, May 31, 2013

The A128T Resistance Mutation Reveals Aberrant Protein Multimerization as the Primary Mechanism of Action of Allosteric HIV-1 Integrase Inhibitors*[S]

Received for publication, December 7, 2012, and in revised form, April 8, 2013 Published, JBC Papers in Press, April 24, 2013, DOI 10.1074/jbc.M112.443390

Lei Feng[‡], Amit Sharma[‡], Alison Slaughter[‡], Nivedita Jena[§], Yasuhiro Koh[¶], Nikolozi Shkriabai[‡], Ross C. Larue[‡], Pratiq A. Patel[§], Hiroaki Mitsuya[¶], Jacques J. Kessl[‡], Alan Engelman[‖], James R. Fuchs[§], and Mamuka Kvaratskhelia[‡1]

From the [‡]Center for Retrovirus Research and Comprehensive Cancer Center and the [§]Division of Medicinal Chemistry and Pharmacognosy, College of Pharmacy, The Ohio State University, Columbus, Ohio 43210, the [¶]Departments of Hematology and Infectious Diseases, Kumamoto University School of Medicine, Kumamoto 860-8556, Japan, and the [‖]Department of Cancer Immunology and AIDS, Dana-Farber Cancer Institute, and Department of Medicine, Harvard Medical School, Boston, Massachusetts 02215

Background: The A128T substitution in HIV-1 integrase (IN) confers resistance to allosteric integrase inhibitors (ALLINIs).
Results: The A128T substitution does not significantly alter ALLINI IC_{50} values for IN-LEDGF/p75 binding but confers marked resistance to ALLINI-induced aberrant integrase multimerization.
Conclusion: Allosteric perturbation of HIV-1 integrase multimerization underlies ALLINI antiviral activity.
Significance: Our findings underscore the mechanism of ALLINI action and will facilitate development of second-generation compounds.

Allosteric HIV-1 integrase (IN) inhibitors (ALLINIs) are a very promising new class of anti-HIV-1 agents that exhibit a multimodal mechanism of action by allosterically modulating IN multimerization and interfering with IN-lens epithelium-derived growth factor (LEDGF)/p75 binding. Selection of viral strains under ALLINI pressure has revealed an A128T substitution in HIV-1 IN as a primary mechanism of resistance. Here, we elucidated the structural and mechanistic basis for this resistance. The A128T substitution did not affect the hydrogen bonding between ALLINI and IN that mimics the IN-LEDGF/p75 interaction but instead altered the positioning of the inhibitor at the IN dimer interface. Consequently, the A128T substitution had only a minor effect on the ALLINI IC_{50} values for IN-LEDGF/p75 binding. Instead, ALLINIs markedly altered the multimerization of IN by promoting aberrant higher order WT (but not A128T) IN oligomers. Accordingly, WT IN catalytic activities and HIV-1 replication were potently inhibited by ALLINIs, whereas the A128T substitution in IN resulted in significant resistance to the inhibitors both *in vitro* and in cell culture assays. The differential multimerization of WT and A128T INs induced by ALLINIs correlated with the differences in infectivity of HIV-1 progeny virions. We conclude that ALLINIs primarily target IN multimerization rather than IN-LEDGF/p75 binding. Our findings provide the structural foundations for developing improved ALLINIs with increased potency and decreased potential to select for drug resistance.

HIV-1 integrase (IN)[2] is an important therapeutic target, as its function is essential for viral replication (1). IN catalyzes the insertion of the reverse-transcribed RNA genome into human chromatin in a two-step reaction (2). During the initial step (termed 3′-processing), IN removes a GT dinucleotide from each 3′ terminus of the viral DNA. The subsequent transesterification reactions (termed DNA strand transfer) covalently join the recessed viral DNA ends into the host genome. To carry out these reactions, highly dynamic IN subunits assemble in the presence of cognate DNA to form the stable synaptic complex or intasome (3–5). Premature multimerization of HIV-1 IN by various ligands in the absence of cognate DNA restricts the functionally essential dynamic interplay between individual subunits and DNA and thus impairs IN catalytic activities (3, 4, 6, 7).

A cellular protein, lens epithelium-derived growth factor (LEDGF)/p75, markedly enhances the integration process *in vitro* and in infected cells. LEDGF/p75 tethers stable synaptic complexes to chromatin via direct interactions of its N-terminal chromatin-binding domain with nucleosomes, whereas its C-terminal IN-binding domain links to HIV-1 IN (8, 9). Structural studies (10, 11) have elucidated the principal interacting interfaces between the LEDGF/p75 IN-binding domain and the HIV-1 IN catalytic core domain (CCD). The cornerstone of this protein-protein interaction is a hydrogen bonding network between the side chain oxygen atoms of LEDGF/p75 Asp-366

* This work was supported, in whole or in part, by National Institutes of Health Grants AI081581 and AI062520 (to M. K.), GM103368 (to A. E. and M. K.), AI097044 (to J. J. K. and J. R. F.).
[S] This article contains supplemental "Experimental Procedures," Figs. S1–S8, Tables 1–6, and additional references.
The atomic coordinates and structure factors (codes 4JLH, 4GW6, and 4GVM) have been deposited in the Protein Data Bank (http://wwpdb.org/).
[1] To whom correspondence should be addressed: Center for Retrovirus Research and Comprehensive Cancer Center, College of Pharmacy, The Ohio State University, 500 West 12th Ave., Columbus, OH 43210. Tel.: 614-292-6091; E-mail: kvaratskhelia.1@osu.edu.

[2] The abbreviations used are: IN, integrase; LEDGF, lens epithelium-derived growth factor; CCD, catalytic core domain; ALLINI, allosteric IN inhibitor; RAL, raltegravir; HTRF, homogeneous time-resolved fluorescence.

and the IN backbone amides of Glu-170 and His-171 (10, 11). These findings have opened up new venues for antiviral drug discovery.

Using a structure-based rational drug design approach, Christ *et al.* (12) developed 2-(quinolin-3-yl)acetic acid derivatives, which inhibit the IN-LEDGF/p75 interaction *in vitro* and HIV-1 replication in cell culture. Paradoxically, the identical class of compounds has emerged from a high-throughput screen for IN 3′-processing activity (13). Subsequent studies from our group and others demonstrated that 2-(quinolin-3-yl)acetic acid derivatives exhibit a multimodal mechanism of action by allosterically modulating the IN structure, which affects both IN-LEDGF/p75 binding and catalytic activity (14–16). Accordingly, we have proposed to name this class of inhibitors as allosteric IN inhibitors (ALLINIs). Structural studies have shown that the carboxylic acid of ALLINIs hydrogen bonds with the backbone amides of Glu-170 and His-171 and thus occupy the principal LEDGF/p75-binding interface (12, 14, 16). At the same time, the quinoline core and the substituted phenyl group of the inhibitor bridge the two IN subunits and promote allosteric multimerization of the protein. As a result, ALLINIs potently inhibit both IN-LEDGF/p75 binding and LEDGF/p75-independent IN catalytic activities.

The ability of ALLINIs to impair steps in the viral replication cycle that extend beyond IN catalytic function results in a highly cooperative inhibition of HIV-1 replication (14). Along these lines, it was recently reported that HIV-1 particles made in the presence of ALLINIs are noninfectious (15). Whereas the Food and Drug Administration-approved HIV-1 IN strand transfer inhibitor raltegravir (RAL) exhibits a Hill coefficient of 1, which is consistent with only a single or non-cooperative mode of action, ALLINIs impair viral replication with a Hill coefficient of ~4, indicating a highly cooperative mode of action (14). Compounds with a high cooperativity are particularly desirable for superior clinical outcomes because they enable stronger viral suppression at clinical drug concentrations (17, 18).

The A128T substitution in HIV-1 IN has been identified from cell culture assays as a primary mechanism for resistance to ALLINI compounds (12, 16, 19). Ala-128 is located at the IN dimer interface in the pocket occupied by ALLINIs or LEDGF/p75. Here, we have investigated the structural and mechanistic properties for the resistance of A128T IN to ALLINIs. Strikingly, the A128T substitution only modestly affected ALLINI IC_{50} values for IN-LEDGF/p75 binding but markedly altered the multimerization of IN in the presence of the inhibitors. As a result, the catalytic activities of the WT protein were potently inhibited by ALLINIs, whereas A128T IN exhibited significant resistance to the inhibitor. Furthermore, considerably higher concentrations of ALLINIs were required to inhibit the infectivity of the A128T mutant virus compared with the WT counterpart. Taken together, our studies highlight that aberrant IN multimerization is the primary target of this class of inhibitors and thus provide the structural foundations for the development of second-generation ALLINIs with increased potency and decreased potential to select for drug resistance.

EXPERIMENTAL PROCEDURES

Antiviral Compounds—ALLINI-1, referred to as BI-1001 previously, was synthesized as described (14). The synthesis of ALLINI-2 is described in supplemental Figs. S1 and S2. RAL and saquinavir were obtained from the National Institutes of Health AIDS Research and Reference Reagent Program.

Expression and Purification of Recombinant Proteins—LEDGF/p75 and WT and A128T HIV-1 IN recombinant proteins with His or FLAG tags were expressed in *Escherichia coli* and purified as described previously (14).

Protein-Protein Interaction Assays—Homogeneous time-resolved fluorescence (HTRF)-based IN-LEDGF/p75 binding and IN multimerization assays were performed as described previously (14). The HTRF signal was recorded using a PerkinElmer EnSpire multimode plate reader.

Solubility Assays—WT IN was diluted to a final concentration of 100 nM in buffer containing 25 mM Tris (pH 7.4), 2 mM $MgCl_2$, 0.1% Nonidet P-40, 1 mg/ml BSA, and either 150 or 750 mM NaCl. Increasing concentrations of ALLINI-1 or ALLINI-2 were then added to the mixture and incubated for 1 h at room temperature. The mixture was subjected to centrifugation for 2 min at 2000 × *g*. The supernatant was collected, and the pellet was washed three times with the same buffer. The supernatant and pellet fractions were analyzed by SDS-PAGE, and IN was detected with anti-His antibody (Abcam).

3′-Processing, Strand Transfer, and LEDGF/p75-dependent Integration Assays—Gel-based LEDGF/p75-dependent and LEDGF/p75-independent integration activity assays were performed as described previously (14). A recently reported time-resolved fluorescence assay (16) was used to quantify IN 3′-processing and strand transfer activities. The HTRF-based LEDGF/p75-dependent integration activity was measured by adding recombinant LEDGF/p75 protein to the assay mixture prior to the incubation with labeled DNA substrates. The time-resolved fluorescence signal was recorded using a PerkinElmer EnSpire multimode plate reader.

Size Exclusion Chromatography—Experiments were performed with a Superdex 200 10/300 GL column (GE Healthcare) at 0.5 ml/min in elution buffer containing 20 mM HEPES (pH 6.8), 750 mM NaCl, 10 mM $MgSO_4$, 0.2 mM EDTA, 5 mM β-mercaptoethanol, 5% glycerol, and 200 μM $ZnCl_2$. IN (20 μM) was incubated with ALLINIs or Me_2SO (control) for 30 min and then subjected to size exclusion chromatography. The column was calibrated with the following proteins: bovine thyroglobulin (670,000 Da), bovine γ-globulin (158,000 Da), chicken ovalbumin (44,000 Da), horse myoglobin (17,000 Da), and vitamin B_{12} (1,350 Da). Proteins were detected by absorbance at 280 nm. All the procedures were performed at 4 °C.

Crystallization and X-ray Structure Determination—The HIV-1 IN CCD (residues 50–212 containing the F185K substitution) and A128T CCD (with an extra substitution of A128T) were expressed and purified as described (20). The CCD was concentrated to 8 mg/ml and crystallized at 4 °C using the hanging drop vapor diffusion method. The crystallization buffer contained 10% PEG 8000, 0.1 M sodium cacodylate (pH 6.5), 0.1 M ammonium sulfate, and 5 mM DTT. Crystals reached 0.1–0.2 mm within 4 weeks. The A128T CCD was concen-

trated to 8.5 mg/ml and crystallized at room temperature (20 °C) using the hanging drop vapor diffusion method. The crystallization buffer contained 0.1 M sodium cacodylate (pH 6.5), 1.4 M sodium acetate, and 5 mM DTT. The crystals reached 0.2–0.4 mm within 1 week.

A soaking buffer containing 5 mM ALLINI-1 or ALLINI-2 was prepared by dissolving the compound in crystallization buffer supplemented with 10% Me_2SO. The protein crystal was soaked in the buffer for 8 h before flash-freezing in liquid N_2. Diffraction data were collected at 100 F on a Rigaku R-AXIS 4++ image plate detector at the Ohio State University Crystallography Facility. Intensity data integration and reduction were performed using the HKL2000 program (21). The molecular replacement program Phaser (22) in the CCP4 package (23) was used to solve the structure, with the HIV-1 IN CCD structure (Protein Data Bank code 1ITG) (20) serving as starting model. The Coot program (24) was used for the subsequent refinement and building of the structure. Refmac5 (25) of the CCP4 package was used for the restraint refinement. TLS (26) and restraint refinement was applied for the last step of the refinement. The crystals belonged to space group $P3_121$ with cell dimensions $a = b = 73$ and $c = 65$ Å, with one 18-kDa monomer in the asymmetric unit. The data collection and refinement statistics are listed in supplemental Table 1. Coordinates have been deposited in the Protein Data Bank with accession numbers 4JLH, 4GW6, and 4GVM (supplemental Table 1).

HIV-1 Virion Production and Infectivity Assay—HEK293T and HeLa TZM-bl cells were cultured in Dulbecco's modified Eagles medium (Invitrogen), 10% FBS (Invitrogen), and 1% antibiotic/antimycotic (Invitrogen) at 37 °C and 5% CO_2. Cultures of HEK293T cells (2×10^5 cells/well of a 6-well plate in 2 ml of complete medium) were transfected with 2 μg of pNL4–3 (WT or A128T mutant) at a 1:3 ratio of DNA to X-tremeGENE HP (Roche Applied Science) following the manufacturer's protocol. Twenty-four hours post-transfection, cells were washed once with complete medium, and the culture supernatant was replaced with complete medium containing Me_2SO, RAL (250 nM), ALLINI-1, or ALLINI-2 (at the indicated concentrations). After 1 h, the culture supernatant was again replaced with fresh complete medium containing either Me_2SO or the indicated inhibitors. The virus-containing cell-free supernatant was collected after 24 h, and HIV-1 Gag p24 ELISA (ZeptoMetrix) was performed following the manufacturer's protocol. Virions equivalent to 2–4 ng of HIV-1 p24 was used to infect 2×10^5 HeLa TZM-bl cells in the presence of 8 μg/ml Polybrene (Sigma). HeLa TZM-bl cultures were extracted in 1× reporter lysis buffer (Promega), and virion infectivity was measured using the luciferase assay (Promega).

Antiviral Activity Assays—ALLINI EC_{50} values were determined in spreading HIV-1 replication assays as described previously (14).

RESULTS

To examine the effects of the A128T substitution on HIV-1 IN function, we compared the catalytic activities of purified recombinant WT and mutant proteins. The two proteins exhibited comparable levels of LEDGF/p75-independent and LEDGF/p75-dependent integration activities (Fig. 1). Thus, the

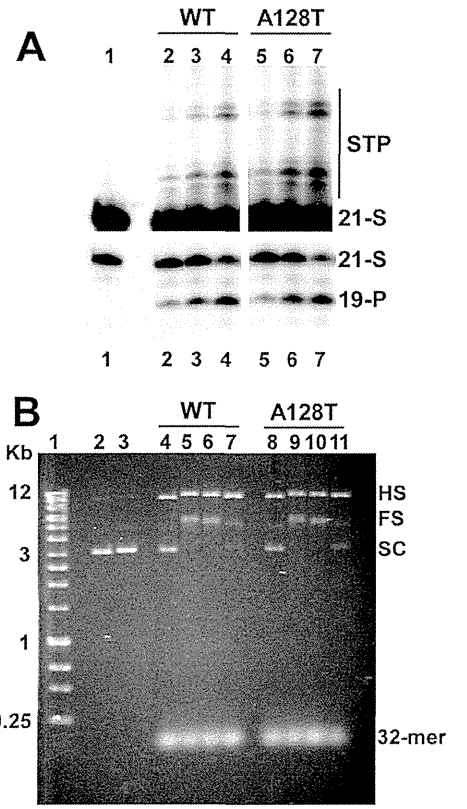

FIGURE 1. **Catalytic activities of WT and A128T INs.** *A*, strand transfer reaction products (*STP; upper panels*) and 3′-processing products (*19-P; lower panels*). *Lane 1*, 21-mer DNA substrate (*21-S*) without IN; *lanes 2–4*, increasing concentrations (0.5, 1, and 2 μM) of WT IN added to the reactions; *lanes 5–7*, increasing concentrations (0.5, 1, and 2 μM) of A128T IN added to the reactions. *B*, concerted integration results. The positions of 32-mer donor and supercoiled (*SC*) target DNA substrates, as well as full-site (*FS*) and half-site (*HS*) integration products, are indicated. *Lane 1*, DNA markers (Bioline Quanti-Marker, 1 kb); *lanes 2* and 3, target DNA; *lane 4*, WT IN (2.4 μM) added to donor and target DNA substrates without LEDGF/p75; *lanes 5–7*, LEDGF/p75 added with decreasing concentrations (2.4, 1.2, and 0.6 μM) of WT IN; *lane 8*, A128T IN (2.4 μM) added to donor and target DNA substrates without LEDGF/p75; *lanes 9–11*, LEDGF/p75 with decreasing concentrations (2.4, 1.2, and 0.6 μM) of A128T IN.

A128T substitution does not significantly alter the function of IN.

The A128T mutation has been shown to confer resistance to four different ALLINI compounds in cell culture assays (12, 15, 16, 19). To delineate the mechanism of drug resistance, the ALLINI-1 and ALLINI-2 compounds were synthesized (Fig. 2). ALLINI-1 was identified by Boehringer Ingelheim through a high-throughput screen for IN 3′-processing activity (13), and its multimodal mechanism of action has been elucidated by our group (14). In resistance studies under selective pressure of ALLINI-1 (19), the A128T substitution in IN was identified in both early and late stage viral passages. This single amino acid change resulted in 32-fold higher ALLINI-1 IC_{50} values compared with the WT virus. In this study, we also examined ALLINI-2, a *tert*-butyl derivative of ALLINI-1. Similar to a published report (16) showing that the *tert*-butyl group increases the potency of this class of compounds, ALLINI-2 was ~10-fold more potent ($IC_{50} = 0.63 \pm 0.3$ μM) (supplemental Table 2) than ALLIN-1 ($IC_{50} = 5.8 \pm 0.1$ μM). Although we have not

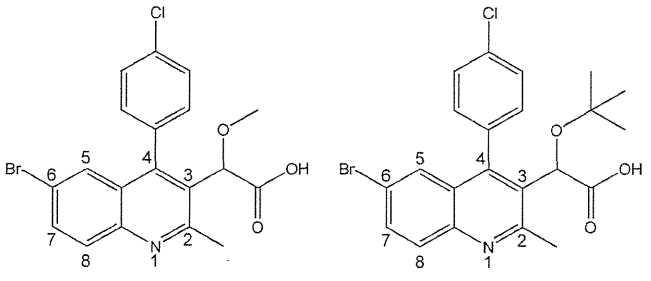

FIGURE 2. **Chemical structures of ALLINI-1 and ALLINI-2.**

selected for the A128T mutation by serially passaging HIV-1 in the presence of ALLINI-2, the ability of this mutation to confer relative pan-tropic resistance to a number of different compounds, including those that harbor the *tert*-butyl moiety (15, 16), gave us confidence that A128T would likely confer resistance to ALLINI-2. Supplemental Table 2 indeed shows that A128T conferred 19-fold resistance to ALLINI-2 in a spreading HIV-1 replication assay.

We and others have shown that ALLINIs inhibit multiple functions of WT IN, including LEDGF/p75-independent catalysis and IN-IN multimerization, with similar IC_{50} values (14–16). Such a mechanism has been attributed to the fact that these compounds occupy the LEDGF/p75-binding pocket at the IN dimer interface. As a result, ALLINIs inhibit IN-LEDGF/p75 binding and also bridge two IN subunits and allosterically modulate their multimerization. In turn, the latter impairs the catalytic functions of WT IN.

Strikingly, we observed that the A128T substitution had markedly different effects on the IC_{50} values for different assays in comparison with WT IN (Table 1). For example, the mutation conferred only an ~2-fold increase in IC_{50} values for inhibiting the IN-LEDGF/p75 interaction, whereas the IC_{50} values for the 3′-processing reaction increased by 287-fold and 1112-fold for ALLINI-1 and ALLINI-2, respectively. Thus, A128T IN was markedly resistant to ALLINIs in 3′-processing reactions, whereas these compounds remained potent inhibitors of A128T IN binding to LEDGF/p75 (Fig. 3 and supplemental Fig. S3). The A128T substitution resulted in ~11.5- and 5-fold resistance to ALLINI-1 and ALLINI-2, respectively, in the strand transfer reactions (Table 1). In LEDGF/p75-dependent integration assays, the mutant protein exhibited ~12- and 25-fold resistance to ALLINI-1 and ALLINI-2, respectively (Table 1).

Interestingly, IN multimerization assays have revealed further striking differences between WT and mutant INs (Fig. 4 and supplemental Fig. S4). Both WT and A128T INs exhibited a characteristic biphasic dose-response curve upon the addition of ALLINIs. The HTRF signal increase with increasing concentrations of inhibitor was due to the inhibitor-induced protein multimerization, yielding higher FRET. Although the exact nature of the descending curve was not clear, it could be explained by reduced accessibility of the fluorescent antibodies to their respective tags in the context of higher order IN oligomers. The assay uses anti-His_6-XL665 and anti-FLAG-europium-cryptate antibodies to monitor fluorescence energy transfer (HTRF signal) between His-IN and IN-FLAG proteins. During the initial multimerization of IN, when dimers and tetramers form, the affinity tags are sufficiently exposed to readily engage the antibodies. However, these interactions may be limited in higher order IN oligomers (see Fig. 5 and supplemental Fig. S5) due to structural hindrance of the affinity tags and could thus account for the drop in HTRF signal. Fig. 4 and supplemental Fig. S4 show that the dose-dependent addition of ALLINIs to WT and A128T INs yielded different peak heights. These differences could be explained by WT and mutant INs adopting different oligomeric states (see below) or alternative conformations in the presence of the inhibitor.

To delineate between these possibilities, we performed size exclusion chromatography experiments (Fig. 5 and supplemental Fig. S5). Due to the reduced sensitivity of this approach compared with the HTRF-based assays, elevated concentrations of IN and ALLINIs were necessary. Tetramer and monomer peaks were detected with both WT and A128T INs in the absence of inhibitor, demonstrating that the substitution does not affect IN multimerization (Fig. 5 and supplemental Fig. S5) or catalytic activities (Fig. 1). Upon the addition of ALLINIs, the tetramer peak of WT IN was markedly reduced, and instead, new peaks corresponding to higher order oligomers were detected. In sharp contrast, the tetramer peak persisted upon the addition of ALLINI-1 or ALLINI-2 to A128T IN (Fig. 5 and supplemental Fig. S5 and Tables 3–6). These findings are consistent with the results of the HTRF-based multimerization assays: the formation of higher order structures upon ALLINI addition resulted in greater HTRF signal strength compared with mutant IN and could also account for the downward slope of the WT IN curves at high compound concentrations (Fig. 4 and supplemental Fig. S4).

We next examined whether the addition of ALLINIs to IN might promote the formation of insoluble aggregates. WT IN was incubated with increasing concentrations of ALLINI-1 or ALLINI-2 and then subjected to centrifugation. The results in Fig. 6 and supplemental Fig. S6 show that, under our reaction conditions, the IN-ALLINI complexes remained soluble. The solubility (Fig. 6 and supplemental Fig. S6) and HTRF-based IN multimerization (Fig. 4 and supplemental Fig. S4) assays were carried out at two different NaCl concentrations (150 and 750 mM) and yielded very similar results, indicating that the changes in the ionic strength of the buffer did not significantly affect the solubility of ALLINI-induced higher order IN oligomers. This supports the notion that higher order IN multimerization and not precipitation led to the decrease in HTRF signal seen in Fig. 4 and supplemental Fig. S4.

To elucidate the structural basis for how the resistance mutation affects ALLINI binding, we solved the crystal structures of the inhibitors bound to the WT and A128T IN CCDs (Fig. 7 and supplemental Fig. S7). The overlay of these two structures shows that the hydrogen bonding network between ALLINIs and subunit 1 is fully preserved in both the WT and mutant proteins (Fig. 7 and supplemental Fig. S7). These include the interactions of the carboxylic acid with the backbone amides of Glu-170 and His-171 and the methoxy group of ALLINI-2 with the side chain of Thr-174. Thus, ALLINIs effectively shield the access of the key LEDGF/p75 Asp-366 contact to its cognate

TABLE 1

Effects of the A128T substitution on the IC_{50} values of ALLINIs

Means ± S.E. are shown for at least three independent experiments, with -fold changes in ALLINI resistance for the mutant enzyme in parentheses.

	IC_{50}							
	IN-LEDGF binding		3′-Processing		Stand transfer		LEDGF-dependent integration	
	WT	A128T	WT	A128T	WT	A128T	WT	A128T
	μM							
ALLINI-1	1.9 ± 0.5	4.0 ± 0.6 (2)	0.91 ± 0.06	261.5 ± 48 (287)	0.4 ± 0.09	4.61 ± 0.45 (11.5)	1.29 ± 0.34	15.6 ± 3.5 (12)
ALLINI-2	0.3 ± 0.02	0.78 ± 0.06 (2.6)	0.18 ± 0.02	200.2 ± 17 (1112)	0.17 ± 0.03	0.89 ± 0.19 (5)	0.06 ± 0.01	1.49 ± 0.03 (25)

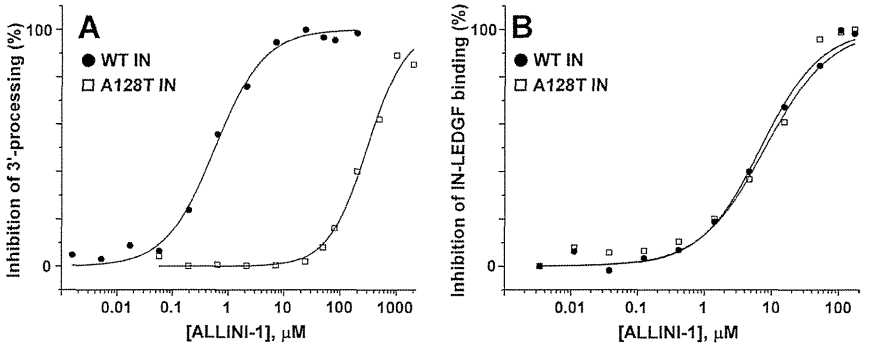

FIGURE 3. ***Effects of ALLINI-1 on 3′-processing activities and IN-LEDGF/p75 binding of WT and A128T INs.*** *A*, dose-response effects of ALLINI-1 on 3′-processing activities of WT (●) and A128T (□) INs. *B*, dose-response effects of ALLINI-1 on the IN-LEDGF/p75 binding for WT (●) and A128T (□) INs. The IC_{50} values and S.E. obtained from curve fittings are given in Table 1.

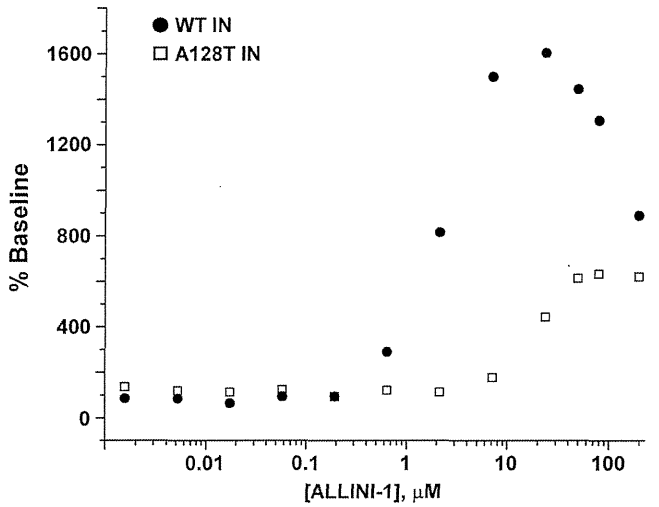

FIGURE 4. **Effects of ALLINI-1 on multimerization of WT and A128T INs.** Shown are the dose-response effects of ALLINI-1-induced multimerization of WT (●) and A128T (□) INs. The HTRF signal observed due to the dynamic exchange of IN subunits in the absence of the inhibitor is considered 100% base line. The mean values of three independent experiments are shown.

hydrogen bonding partners on both WT and A128T INs. Accordingly, these compounds inhibited the binding of the cellular cofactor to WT and A128T INs with comparable IC_{50} values (Fig. 3 and supplemental Fig. S3).

Interestingly, the A128T substitution affected the positioning of the quinoline group (Fig. 7 and supplemental Fig. S7). ALLINIs were shifted down and inward (toward the protein) by ~2 Å as measured at the common bromine atom. Because the positioning of the carboxylic group remained intact, this resulted in the rotation of the rigid molecule by ~18° (as measured by the shift of the bromine atom with respect to the C3 atom (numbering according to Fig. 2) in the quinoline ring). This change also caused the substituted phenyl group to shift downward by 0.8 Å at the chlorine atom. These structural changes could be explained by the substitution of Ala-128 with the bulkier and polar threonine, which could exert a steric effect and electronic repulsion of the compounds. The shifts of the quinoline and substituted phenyl groups that bridge the two monomers of the CCD could be the reason for the differential multimerization of WT and mutant INs.

A previous study (15) demonstrated that ALLINIs do not affect bulk viral particle production but nevertheless impair the infectivity of HIV-1 progeny virions. Here, we examined how the A128T substitution affects this aspect of ALLINI inhibition (Fig. 8 and supplemental Fig. S8). For this, HEK293T cells were transfected with pNL4–3 (WT or A128T mutant) and cultured for 24 h to ensure expression of the provirus. Next, we monitored the production of HIV-1 particles in the presence of increasing concentrations of ALLINIs. Twenty-four hours post-addition of the compounds, the virus-containing cell-free supernatant was harvested, and the amounts of viral particles produced were measured by p24 ELISA. The production of both WT and A128T IN viral particles was not affected by ALLINIs (Fig. 8 (*upper panel*) and supplemental Fig. S8*A*). Subsequently, we examined the infectivity of these progeny virions in a HeLa-based reporter cell line (TZM-bl) containing the HIV-1 LTR-luciferase reporter gene. For this, TZM-bl cells were infected with equivalent cell-free virions without any additional inhibitor being added to the target cells. Under these conditions, only 0.1% of the input ALLINIs was carried over from the producer cells to the target cells based on the supernatant volumes used for the infections. At the highest concentration of ALLINIs tested (100 μM ALLINI-1 treatment of the producer cells), only 100 nM inhibitor would carry over, which is well below the IC_{50} value for the WT virus and thus will have

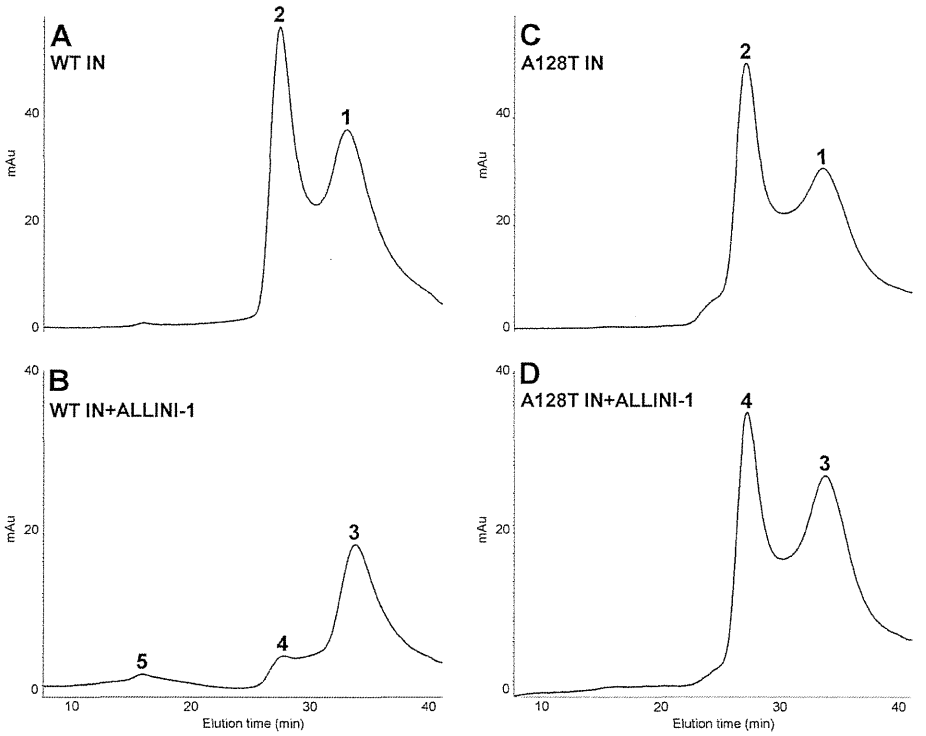

FIGURE 5. **Size exclusion chromatography demonstrating differential multimerization of WT and A128T INs in the presence of ALLINI-1.** Shown are the elution profiles of 20 μM WT IN in the absence (*A*) and presence (*B*) of 80 μM ALLINI-1. The elution times and respective estimated oligomeric states for the indicated peak are summarized in supplemental Table 3. Also shown are the elution profiles of 20 μM A128T IN in the absence (*C*) and presence (*D*) of 80 μM ALLINI-1. The elution times and respective estimated oligomeric states of A128T peaks are summarized in supplemental Table 4.

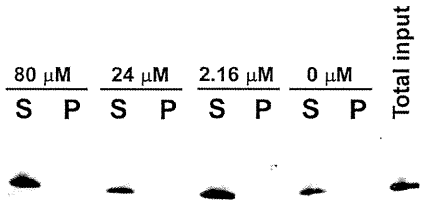

FIGURE 6. **Solubility of the complex of WT IN and ALLINI-1.** WT IN was incubated with the indicated concentrations of ALLINI-1 and then subjected to centrifugation. The supernatant (*S*) and pellet (*P*) fractions were analyzed by SDS-PAGE, and IN was detected by anti-His antibody.

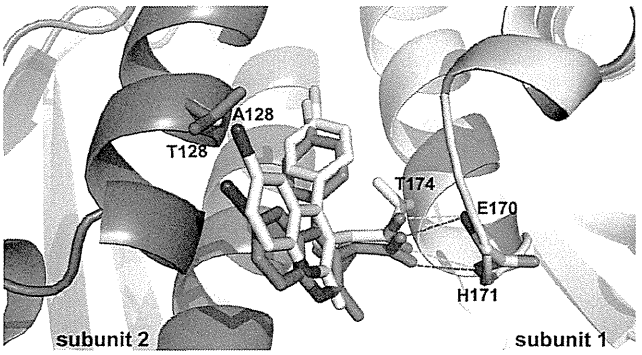

FIGURE 7. **Overlay of crystal structures of ALLINI-1 bound to A128T and WT IN CCDs.** Ala-128 and its corresponding ligand ALLINI-1 are colored *yellow*, whereas Thr-128 and the respective ALLINI-1 molecule are colored *magenta*. Hydrogen bonds between ALLINI-1 molecules and the backbones of Glu-170 and His-171 are shown by *yellow* (for WT IN) and *magenta* (for A128T IN) *dashed lines*. Subunits 1 and 2 are colored *cyan* and *gray*, respectively.

negligible effects on the TZM-bl cell infections. The results in Fig. 8 (*lower panel*) and supplemental Fig. S8*B* demonstrate that WT virions produced in the presence of the inhibitors lost their infectivity, with estimated IC_{50} values of ~6 μM for ALLINI-1 and ~0.5 μM for ALLINI-2. In contrast, the A128T virions exhibited a marked resistance to ALLINIs (Fig. 8 (*lower panel*) and supplemental Fig. S8*B*). Control experiments with RAL showed no effects of this inhibitor on viral production or infectivity (data not shown).

DISCUSSION

ALLINIs are a growing class of new anti-HIV-1 compounds. Importantly, these inhibitors are complementary to all Food and Drug Administration-approved antiretroviral agents, including the IN strand transfer inhibitors RAL and elvitegravir. Whereas the IN strand transfer inhibitors specifically interact with the IN-viral DNA complex (27), ALLINIs target a clinically unexploited IN dimer interface at the LEDGF/p75-binding site. Consequently, ALLINIs allosterically modulate IN multimerization and impair IN-LEDGF/p75 binding (14–16).

The IN A128T substitution has been identified from cell culture assays as a primary mechanism of HIV-1 resistance to numerous ALLINIs (12, 15, 16, 19). Here, we elucidated the structural and mechanistic basis for this resistance. The alanine-to-threonine substitution affects positioning of the core quinoline and substituted phenyl ring of ALLINIs that bridge the two IN subunits, whereas the hydrogen bonding network between the inhibitor and the protein that closely mimics the

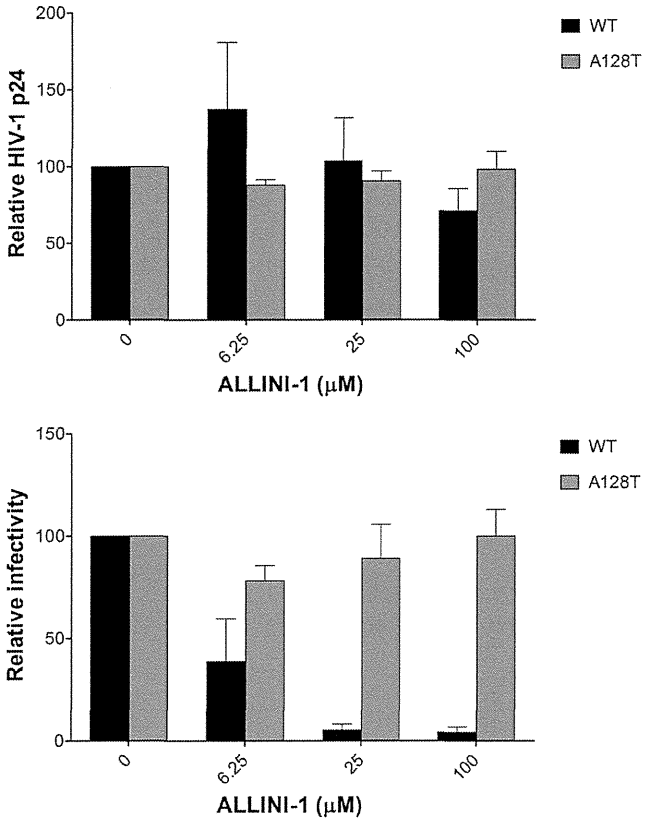

FIGURE 8. **Effects of ALLINI-1 on WT and A128T HIV-1 p24 production and infectivity.** *Upper panel,* HEK293T cells were transfected with either WT or A128T IN provirus. HIV-1 particles were produced in the presence or absence of ALLINI-1 for 24 h, and cell-free Gag was measured by HIV-1 p24 ELISA. *Lower panel,* the indicated WT or A128T IN cell-free virus equivalent to 4 ng of HIV-1 p24 was used to infect TZM-bl cells, and luciferase assay was performed at 48 h post-infection. The luciferase signal, obtained in the absence of ALLINI-1 (Me_2SO alone) for WT or A128T IN, was set to 100%. The average values from at least triplicate infections are shown, and *error bars* represent S.D.

IN-LEDGF/p75 interaction remains intact. As a result, the A128T substitution shows marked resistance to ALLINI-induced aberrant multimerization of IN compared with its WT counterpart, whereas the compound remains a potent inhibitor of the A128T IN binding to LEDGF/p75.

We have shown that ALLINIs promote aberrant higher order multimerization of WT IN, but not A128T IN. Although previous studies have attributed the HTRF signal increase to IN dimerization (16), the size exclusion chromatography data in Fig. 5 and supplemental Fig. S5 clarify that the addition of ALLINIs to the WT protein promotes the formation of higher order oligomers. As a result, the catalytic activities of the WT protein are fully compromised. In sharp contrast, A128T IN is remarkably resistant to ALLINIs in the 3′-processing assays (287- and 1112-fold for ALLINI-1 and ALLINI-2, respectively) and exhibits 5–11-fold resistance in strand transfer assays. How does one explain the differential levels of resistance of A128T IN for 3′-processing and strand transfer activities? The HTRF assays coupled with size exclusion chromatography indicate that ALLINIs stabilize a tetrameric form of A128T IN. Of note, IN tetramers formed in the absence and presence of viral DNA adopt distinct conformations (3). Although preformed tetramers are known to be active in 3′-processing, the strand transfer reactions require individual IN monomers to assemble in the presence of viral DNA to correctly engage target DNA (3, 4). Parallels can be drawn with our earlier results demonstrating the importance of highly dynamic interplay of individual IN subunits for productive integration (3, 4). The IN tetramers stabilized by the LEDGF/p75 IN-binding domain are active in 3′-processing reactions but fail to catalyze concerted HIV-1 integration. Similarly, IN tetramers prematurely stabilized by ALLINIs are likely to be different from the fully functional tetramers in the intasome formed in the presence of DNA substrate.

To understand the 5–11-fold resistance of A128T IN in the strand transfer assays, we analyzed the HTRF data in Fig. 4 and supplemental Fig. S4. Accurate measurements of ALLINI IC_{50} values from these assays were complicated due to biphasic curves and differing peak heights for WT and A128T INs. Still, the analysis of the initial ascending curves enabled us to estimate the IC_{50} values for WT *versus* A128T IN: 2.27 ± 0.13 μM *versus* 17.81 ± 1.46 μM for ALLINI-1 and 0.070 ± 0.008 μM *versus* 0.68 ± 0.06 μM for ALLINI-2. The ~10-fold increase in estimated IC_{50} values for the initial multimerization phase for A128T IN compared with its WT counterpart could explain the observed resistance of mutant IN in the strand transfer assays (Table 1).

The differential multimerization of WT and A128T INs induced by ALLINIs correlates with the differences in infectivity of HIV-1 progeny virions. The treatment of producer cells with the inhibitors impairs WT HIV-1 infectivity, with estimated IC_{50} values of ~6 μM for ALLINI-1 and ~0.6 μM for ALLINI-2, whereas A128T HIV-1 exhibits marked resistance to these compounds (Fig. 8 and supplemental Fig. S8). In turn, these results correlate well with the inhibitory activities of these compounds with respect to WT and A128T HIV-1 replication in spreading assays (supplemental Table 2) (14).

In conclusion, our findings that the A128T substitution did not significantly alter ALLINI IC_{50} values for IN-LEDGF/p75 binding but substantially affected IN multimerization in the presence of the inhibitors indicate that allosteric IN oligomerization is the primary target of these inhibitors in infected cells. Our structural data showing that the A128T substitution repositions the quinoline ring of ALLINIs at the IN dimer interface provide a path for rationale development of second-generation ALLINI compounds with decreased potential to select for drug resistance.

REFERENCES

1. Johnson, A. A., Marchand, C., and Pommier, Y. (2004) HIV-1 integrase inhibitors: a decade of research and two drugs in clinical trial. *Curr. Top. Med. Chem.* **4,** 1059–1077
2. Brown, P. O. (1997) Integration. in *Retroviruses* (Coffin, J. M., Hughes, S. H., and Varmus, H. E. eds) pp. 161–204, Cold Spring Harbor Laboratory, Plainview, NY
3. Kessl, J. J., Li, M., Ignatov, M., Shkriabai, N., Eidahl, J. O., Feng, L., Musier-Forsyth, K., Craigie, R., and Kvaratskhelia, M. (2011) FRET analysis reveals distinct conformations of IN tetramers in the presence of viral DNA or LEDGF/p75. *Nucleic Acids Res.* **39,** 9009–9022
4. McKee, C. J., Kessl, J. J., Shkriabai, N., Dar, M. J., Engelman, A., and Kvaratskhelia, M. (2008) Dynamic modulation of HIV-1 integrase structure and function by cellular lens epithelium-derived growth factor (LEDGF)

protein. *J. Biol. Chem.* **283,** 31802–31812
5. Li, M., Mizuuchi, M., Burke, T. R., Jr., and Craigie, R. (2006) Retroviral DNA integration: reaction pathway and critical intermediates. *EMBO J.* **25,** 1295–1304
6. Kessl, J. J., Eidahl, J. O., Shkriabai, N., Zhao, Z., McKee, C. J., Hess, S., Burke, T. R., Jr., and Kvaratskhelia, M. (2009) An allosteric mechanism for inhibiting HIV-1 integrase with a small molecule. *Mol. Pharmacol.* **76,** 824–832
7. Raghavendra, N. K., and Engelman, A. (2007) LEDGF/p75 interferes with the formation of synaptic nucleoprotein complexes that catalyze full-site HIV-1 DNA integration *in vitro*: implications for the mechanism of viral cDNA integration. *Virology* **360,** 1–5
8. Maertens, G., Cherepanov, P., Pluymers, W., Busschots, K., De Clercq, E., Debyser, Z., and Engelborghs, Y. (2003) LEDGF/p75 is essential for nuclear and chromosomal targeting of HIV-1 integrase in human cells. *J. Biol. Chem.* **278,** 33528–33539
9. Cherepanov, P., Devroe, E., Silver, P. A., and Engelman, A. (2004) Identification of an evolutionarily conserved domain in human lens epithelium-derived growth factor/transcriptional co-activator p75 (LEDGF/p75) that binds HIV-1 integrase. *J. Biol. Chem.* **279,** 48883–48892
10. Hare, S., Shun, M. C., Gupta, S. S., Valkov, E., Engelman, A., and Cherepanov, P. (2009) A novel co-crystal structure affords the design of gain-of-function lentiviral integrase mutants in the presence of modified PSIP1/LEDGF/p75. *PLoS Pathog.* **5,** e1000259
11. Cherepanov, P., Ambrosio, A. L., Rahman, S., Ellenberger, T., and Engelman, A. (2005) Structural basis for the recognition between HIV-1 integrase and transcriptional coactivator p75. *Proc. Natl. Acad. Sci. U.S.A.* **102,** 17308–17313
12. Christ, F., Voet, A., Marchand, A., Nicolet, S., Desimmie, B. A., Marchand, D., Bardiot, D., Van der Veken, N. J., Van Remoortel, B., Strelkov, S. V., De Maeyer, M., Chaltin, P., and Debyser, Z. (2010) Rational design of small-molecule inhibitors of the LEDGF/p75-integrase interaction and HIV replication. *Nat. Chem. Biol.* **6,** 442–448
13. Tsantrizos, Y. S., Boes, M., Brochu, C., Fenwick, C., Malenfant, E., Mason, S., Pesant, M. (November 22, 2007) Inhibitors of human immunodeficiency virus replication. International Patent PCT/CA2007/000845
14. Kessl, J. J., Jena, N., Koh, Y., Taskent-Sezgin, H., Slaughter, A., Feng, L., de Silva, S., Wu, L., Le Grice, S. F., Engelman, A., Fuchs, J. R., and Kvaratskhelia, M. (2012) A multimode, cooperative mechanism of action of allosteric HIV-1 integrase inhibitors. *J. Biol. Chem.* **287,** 16801–16811
15. Christ, F., Shaw, S., Demeulemeester, J., Desimmie, B. A., Marchand, A., Butler, S., Smets, W., Chaltin, P., Westby, M., Debyser, Z., and Pickford, C. (2012) Small-molecule inhibitors of the LEDGF/p75 binding site of integrase block HIV replication and modulate integrase multimerization. *Antimicrob. agents Chemother.* **56,** 4365–4374
16. Tsiang, M., Jones, G. S., Niedziela-Majka, A., Kan, E., Lansdon, E. B., Huang, W., Hung, M., Samuel, D., Novikov, N., Xu, Y., Mitchell, M., Guo, H., Babaoglu, K., Liu, X., Geleziunas, R., and Sakowicz, R. (2012) New class of HIV-1 integrase (IN) inhibitors with a dual mode of action. *J. Biol. Chem.* **287,** 21189–21203
17. Shen, L., Rabi, S. A., and Siliciano, R. F. (2009) A novel method for determining the inhibitory potential of anti-HIV drugs. *Trends Pharmacol. Sci.* **30,** 610–616
18. Shen, L., Peterson, S., Sedaghat, A. R., McMahon, M. A., Callender, M., Zhang, H., Zhou, Y., Pitt, E., Anderson, K. S., Acosta, E. P., and Siliciano, R. F. (2008) Dose-response curve slope sets class-specific limits on inhibitory potential of anti-HIV drugs. *Nat. Med.* **14,** 762–766
19. Fenwick, C. W., Tremblay, S., Wardrop, E., Bethell, R., Coulomb, R., Elston, R., Faucher, A.-M., Mason, S., Simoneau, B., Tsantrizos, Y., and Yoakim, C. (2011) Resistance studies with HIV-1 non-catalytic site integrase inhibitors. *International Workshop on HIV and Hepatitis Virus Drug Resistance and Curative Strategies, Los Cabos, Mexico, June 7–11, 2011*
20. Dyda, F., Hickman, A. B., Jenkins, T. M., Engelman, A., Craigie, R., and Davies, D. R. (1994) Crystal structure of the catalytic domain of HIV-1 integrase: similarity to other polynucleotidyl transferases. *Science* **266,** 1981–1986
21. Otwinowski, Z., and Minor, W. (1997) Processing of x-ray diffraction data collected in oscillation mode. *Methods Enzymol.* **276,** 307–326
22. McCoy, A. J., Grosse-Kunstleve, R. W., Adams, P. D., Winn, M. D., Storoni, L. C., and Read, R. J. (2007) Phaser crystallographic software. *J. Appl. Crystallogr.* **40,** 658–674
23. Collaborative Computational Project, Number 4 (1994) The CCP4 suite: programs for protein crystallography. *Acta Crystallogr. D Biol. Crystallogr.* **50,** 760–763
24. Emsley, P., Lohkamp, B., Scott, W. G., and Cowtan, K. (2010) Features and development of Coot. *Acta Crystallogr. D Biol. Crystallogr.* **66,** 486–501
25. Murshudov, G. N., Vagin, A. A., and Dodson, E. J. (1997) Refinement of macromolecular structures by the maximum-likelihood method. *Acta Crystallogr. D Biol. Crystallogr.* **53,** 240–255
26. Painter, J., and Merritt, E. A. (2006) Optimal description of a protein structure in terms of multiple groups undergoing TLS motion. *Acta Crystallogr. D Biol. Crystallogr.* **62,** 439–450
27. Hare, S., Gupta, S. S., Valkov, E., Engelman, A., and Cherepanov, P. (2010) Retroviral intasome assembly and inhibition of DNA strand transfer. *Nature* **464,** 232–236

AAC
Journals.ASM.org

P2′ Benzene Carboxylic Acid Moiety Is Associated with Decrease in Cellular Uptake: Evaluation of Novel Nonpeptidic HIV-1 Protease Inhibitors Containing P2 *bis*-Tetrahydrofuran Moiety

Ravikiran S. Yedidi,[a] Kenji Maeda,[a] W. Sean Fyvie,[b] Melinda Steffey,[b] David A. Davis,[c] Ira Palmer,[d] Manabu Aoki,[e,f] Joshua D. Kaufman,[d] Stephen J. Stahl,[d] Harisha Garimella,[a] Debananda Das,[a] Paul T. Wingfield,[d] Arun K. Ghosh,[b] Hiroaki Mitsuya[a,e]

Experimental Retrovirology Section[a] and Retroviral Disease Section,[c] HIV and AIDS Malignancy Branch, National Cancer Institute, National Institutes of Health, Bethesda, Maryland, USA; Departments of Chemistry and Medicinal Chemistry, Purdue University, West Lafayette, Indiana, USA[b]; Protein Expression Laboratory, National Institute of Arthritis and Musculoskeletal and Skin Diseases, National Institutes of Health, Bethesda, Maryland, USA[d]; Departments of Hematology and Infectious Diseases, Kumamoto University Graduate School of Biomedical Sciences, Kumamoto, Japan[e]; Department of Medical Technology, Kumamoto Health Science University, Kumamoto, Japan[f]

GRL007 and GRL008, two structurally related nonpeptidic human immunodeficiency virus type 1 (HIV-1) protease inhibitors (PIs) containing 3(*R*),3a(*S*),6a(*R*)-*bis*-tetrahydrofuranylurethane (*bis*-THF) as the P2 moiety and a sulfonamide isostere consisting of benzene carboxylic acid and benzene carboxamide as the P2′ moiety, respectively, were evaluated for their antiviral activity and interactions with wild-type protease (PR^{WT}). Both GRL007 (K_i of 12.7 pM with PR^{WT}) and GRL008 (K_i of 8.9 pM) inhibited PR^{WT} with high potency *in vitro*. X-ray crystallographic analysis of PR^{WT} in complex with GRL007 or GRL008 showed that the *bis*-THF moiety of both compounds has three direct polar contacts with the backbone amide nitrogen atoms of Asp29 and Asp30 of PR^{WT}. The P2′ moiety of both compounds showed one direct contact with the backbone of Asp30′ and a bridging polar contact with Gly48′ through a water molecule. Cell-based antiviral assays showed that GRL007 was inactive (50% effective concentration [EC_{50}] of >1 μM) while GRL008 was highly active (EC_{50} of 0.04 μM) against wild-type HIV-1. High-performance liquid chromatography (HPLC)/mass spectrometry-based cellular uptake assays showed 8.1- and 84-fold higher intracellular concentrations of GRL008 than GRL007 in human MT-2 and MT-4 cell extracts, respectively. Thus, GRL007, in spite of its favorable enzyme-inhibitory activity and protease binding profile, exhibited a lack of antiviral activity in cell-based assays, most likely due to its compromised cellular uptake associated with its P2′ benzene carboxylic acid moiety. The anti-HIV-1 potency, favorable toxicity, and binding profile of GRL008 suggest that further optimization of the P2′ moiety may improve its antiretroviral features.

Over the past 20 years, antiretroviral therapy (ART) has made substantial progress in improving the quality of life and increasing the survival of individuals that are infected with human immunodeficiency virus type 1 (HIV-1). Moreover, ART has recently been shown to block the sexual transmission of HIV-1 very effectively (1). However, it is of note that AIDS caused by HIV-1 infection claimed 1.7 million lives in 2011, according to the latest report from the joint United Nations Programme on HIV/AIDS (UNAIDS [www.unaids.org]). Hence, more efforts are needed to block the spread of HIV-1 infection, to effectively treat HIV-1-infected individuals, and to improve the quality of life of those living with HIV-1 infection.

ART is given as combination chemotherapy using multiple classes of anti-HIV-1 drugs (fusion inhibitors [2], entry inhibitors [3], reverse transcriptase inhibitors [4], integrase inhibitors [5], and protease inhibitors [PIs] [6]) which have been proven to be effective in targeting different stages of viral replication. Among such viral drug targets, HIV-1 protease (PR) is a critical and successful drug target since its role is essential and indispensable for the maturation and infectivity of the virus (7, 8). HIV-1 protease is an aspartyl protease (9) consisting of a pair of identical monomers of 99 amino acids each (10). The error proneness (11) of reverse transcriptase and the rapid replication of HIV-1 are known to be associated with clinical selection of drug-resistant variants (12) that have accumulated mutations in the viral proteins, including protease (13).

Darunavir (DRV) (6), the latest FDA-approved PI, is highly active against drug-resistant variants of HIV-1 (14) and has a dual mechanism of inhibition: (i) enzymatic inhibition and (ii) protease dimerization inhibition (15). DRV has been highly efficacious in suppressing HIV-1 replication and bringing about substantial clinical benefits to individuals infected with HIV-1 (16). However, recent studies have demonstrated that certain individuals who had received long-term ART have failed otherwise would-be effective DRV-containing regimens (17). Indeed, we have successfully generated highly DRV-resistant variants, which can be seen in individuals failing DRV-containing regimens, by using a mixture of multidrug-resistant clinical strains of HIV-1 in test tubes (18). Thus, the development of novel antiretroviral agents that are active against wild-type HIV-1 (HIV^{WT}) and have a high genetic barrier against such DRV-resistant variants is urgently needed.

X-ray crystal structures are widely used to analyze the binding

Received 24 April 2013 Returned for modification 9 May 2013
Accepted 17 July 2013
Published ahead of print 22 July 2013
Address correspondence to Hiroaki Mitsuya, hmitsuya@helix.nih.gov.
Supplemental material for this article may be found at http://dx.doi.org/10.1128/AAC.00868-13.

doi:10.1128/AAC.00868-13

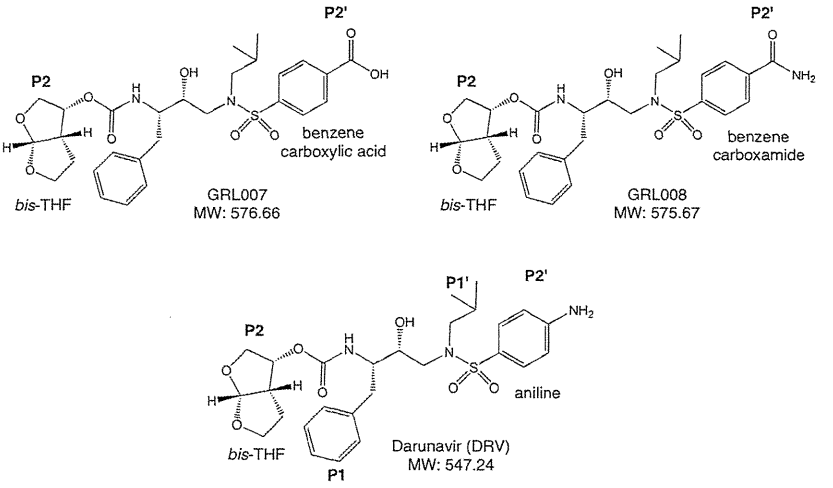

FIG 1 Structures of GRL007, GRL008, and DRV. Structures of GRL007, GRL008, and DRV are shown with the P2 (*bis*-THF) and P2′ moieties labeled. GRL007, GRL008, and DRV contain benzene carboxylic acid, benzene carboxamide, and aniline as P2′ moieties, respectively. All three PIs have a phenyl group at the P1 and an isopropyl group at the P1′ positions with a transition state-mimetic hydroxyl group in between.

interactions of protease inhibitors. In the present study, the crystal structure of DRV in complex with wild-type HIV-1 protease (PR^{WT}) (Protein Data Bank identification code [PDB ID] 4HLA) showed two bridging crystallographic water molecules between the amine group from the P2′ aniline moiety of DRV and backbone amide nitrogen atom of Gly48′. In an effort to develop novel PIs with high genetic barriers, it was hypothesized that modification of the P2′ aniline moiety of DRV with either benzene carboxylic acid or benzene carboxamide would replace one of the two bridging crystallographic water molecules and enhance the binding of the PI to the protease in the S2′ binding pocket while maintaining the polar contact with the backbone of Asp30′. Two structurally related novel nonpeptidic PIs, GRL007 and GRL008, were designed, synthesized, and evaluated for their anti-HIV-1 profiles. GRL007 and GRL008 contain the 3(*R*),3a(*S*),6a(*R*)-*bis*-tetrahydrofuranylurethane (*bis*-THF) group as the P2 moiety (similar to that of DRV) but have benzene carboxylic acid and benzene carboxamide as a P2′ moiety, respectively (Fig. 1). Both compounds were evaluated using *in vitro* enzyme inhibition assays as well as cell-based antiviral assays. Each compound was cocrystallized with wild-type HIV-1 protease (PR^{WT}), the crystal structures were solved, and the interactions were analyzed. Bioavailability is often an issue that plays a critical role in the *in vivo* efficacy of PIs. Hence, the cell permeability of GRL007 and GRL008 was evaluated using a high-performance liquid chromatography/mass spectrometry (HPLC/MS)-based cellular uptake assay.

MATERIALS AND METHODS

Agents, enzyme inhibition assays, and antiviral assays. DRV was synthesized as previously described (19). GRL007 and GRL008 were synthesized by Arun K. Ghosh and coworkers (the details of the synthesis procedures will be published separately). Amprenavir (APV), saquinavir (SQV), and tipranavir (TPV) were provided by the NIH AIDS Research and Reference Reagent Program. Enzyme inhibition constants (K_is) were obtained using enzyme inhibition assays as described previously (6). The HIV^{WT} (HIV-1_{NL4-3} and HIV-1_{LAI}) virus was harvested from the supernatants of chronically infected H9 cells as previously described (14). The viral titers (50% tissue culture infective doses [$TCID_{50}$s]) of the supernatants containing HIV^{WT} were determined using an MTT (3-[4,5-dimethylthiazol-2-yl]-2,5-diphenyl tetrazolium bromide)-based assay. Human MT-2 and MT-4 cells were grown in RPMI 1640 medium (Lonza, Walkersville, MD) with 10% fetal bovine serum (FBS). HIV-1_{LAI} was used to infect human MT-2 cells, while HIV-1_{NL4-3} was used to infect human MT-4 cells. Cells were exposed to 50 $TCID_{50}$s of HIV^{WT} in the presence of different concentrations (ranging from 1 μM to 1 nM) of GRL007, GRL008, or DRV. In the case of GRL007, higher concentrations up to 10 μM were tested in MT-2 cells. DRV was used as a control compound. The FDA-approved PIs APV, SQV, and TPV were also included in the assay. An MTT-based colorimetric assay was performed to determine the number of live cells at each given concentration of drug after exposure to the virus. Assays were conducted in triplicates for each concentration.

Protease expression and purification. The recombinant PR^{WT} (derived from HIV-1_{LAI}) was expressed in *Escherichia coli* strain BL21(DE3), using the T7 expression system as described previously (20). Briefly, the transformants were grown in lysogeny broth (LB) medium at 37°C until the optical density at 600 nm (OD_{600}) reached 0.6. The cells were induced with isopropyl-β-D-1-thiogalactopyranoside (IPTG) at 37°C for 3 h and were harvested by centrifugation (10,000 × *g*) for 30 min. The PR^{WT}-expressing *E. coli* cell pellet was resuspended in a 4:1 (vol/wt) ratio of buffer A (50 mM Tris, pH 7.5, 1 mM EDTA, 2 mM dithiothreitol [DTT]). The cell suspension was lysed by two passes through a French press, followed by 1 min of sonication. The suspension was then centrifuged for 1 h at 25,000 × *g*. The pellet was washed with buffer A containing 1% Triton X-100 and 1 M urea and centrifuged as before. The washed pellet was extracted with 3 M guanidine HCl (GnCl) and centrifuged at 100,000 × *g* for 1 h. The supernatant was loaded on a Sephadex-200 column (60-mm diameter by 600-mm length) that was preequilibrated with 4 M GnCl. The fractions were analyzed by sodium dodecyl sulfate-polyacrylamide gel electrophoresis (SDS-PAGE). The fractions containing PR^{WT} were pooled and loaded onto an HPLC column packed with Source 15 reverse-phase chromatography (RPC) resin. A gradient of 0 to 70% acetonitrile in 0.1% trifluoroacetic acid (TFA) was run to elute the protein. The fractions were analyzed by SDS-PAGE. All the resins were obtained from GE Healthcare Life Sciences (Piscataway, NJ). Purified PR^{WT} aliquots (1 ml each) were stored at −80°C until further use.

Protease refolding. The purified PR^{WT} (~3.5 mg/ml) aliquot (1 ml) in the reverse-phase (RP) pool was thawed on ice, lyophilized, and redissolved in 1 ml of 50% acetic acid solution. Refolding buffer (50 mM sodium acetate, pH 5.2, 5% ethylene glycol, 10% glycerol, 5 mM DTT, and a 5- to 10-fold molar excess of PI) was prepared fresh. The PR^{WT} solution

in 50% acetic acid was added dropwise to 29 ml of refolding buffer with stirring on ice. PR^{WT} was refolded for at least 6 h at 4°C with constant stirring. The refolded PR^{WT}-drug complex was concentrated by centrifugation at 4,000 × *g* using Amicon filters (3-kDa molecular mass cutoff). The final protein concentration was determined to be 1.5 mg/ml.

Crystallization of protease-drug complexes. The hanging-drop vapor diffusion method was used for crystallization of PR^{WT}-drug complex. Equal volumes of PR^{WT}-drug complex and well solution were mixed to a final volume of 8 μl per drop. Diffraction-quality crystals were obtained using 1.6 M ammonium sulfate as a precipitant. Individual rod-shaped crystals were picked up into the nylon loops, which were instantaneously coated with 30% glucose as a cryo-protectant and frozen in liquid nitrogen.

X-ray diffraction data collection and processing. X-ray diffraction data for PR^{WT}-GRL007 and PR^{WT}-GRL008 were collected at beam lines 21-ID and 22-ID, respectively, located at the Advanced Photon Source (APS), Argonne National Laboratory, IL. The data for PR^{WT}-DRV were collected using the RIGAKU X-ray generator. The diffraction data for PR^{WT}-GRL008 were processed and scaled using the HKL2000 program (21), while the data for PR^{WT}-GRL007 and PR^{WT}-DRV were processed using iMOSFLM (22) and scaled using SCALA (23) through the CCP4 (24) interface. Diffraction data processing parameters are shown in Table S1 in the supplemental material.

Crystal structure solutions and refinement. Molecular replacement was performed using MOLREP (25) through the CCP4 interface, with PDB ID 1MUI (without ligand) as a search model. Structure solutions were directly refined using REFMAC5 (26). Initial coordinates for DRV were taken from PDB ID 2IEN. Initial coordinates for GRL007 and GRL008 were prepared by modifying the structure of DRV taken from the crystal structure of PDB ID 2IEN. The molecular models of GRL007 and GRL008 were fit into the electron density using ARP/wARP (27) ligands (28) through the CCP4 interface and manually checked. Refinement libraries for GRL007 and GRL008 were prepared using the PRODRG (29) server. Each drug was fit in two orientations guided by the difference electron density contoured at >2.0 σ, and the occupancies were refined. Solvent molecules were built using the ARP/wARP solvent building module through the CCP4 interface. The stereochemistry of all structures was refined using the interface phenix.refine (30). Refinement statistics for all the structures are shown in Table S2 in the supplemental material. The final refined structures were used for structural analysis. Polar contacts were calculated by using a 3.5-Å-distance cutoff between the heavy atoms (oxygen and nitrogen). Polar contacts with a distance of >3.5 Å were considered weak interactions. Hydrophobic contacts were calculated between two carbon atoms (one from PI and one from PR^{WT}) within a 4-Å distance.

Preparation of MT-2 and MT-4 cell extracts for cellular uptake assays. Cell extracts were prepared as described previously (31). Briefly, 10 million cells were incubated with each drug (50 μM final concentration) at 37°C for 24 h. Cells were harvested and washed with phosphate-buffered saline (PBS) three times, with a 5-ml volume per wash. The final cell pellets were resuspended in 60% methanol solution, and the suspensions were boiled at 95°C for 5 min with shaking. The boiled suspensions were cooled to room temperature and centrifuged at 13,000 rpm for 10 min to separate cell debris from the solvent extract. Supernatants (solvent extracts) were transferred into new tubes, and the solvent was evaporated overnight. Dimethyl sulfoxide (DMSO) (50 μl per tube) was added to the dried tubes, and the tubes were incubated at 37°C for 1 h with shaking. Samples were then analyzed using RP-HPLC/MS.

RP-HPLC/ESI-MS analysis of protease inhibitors. Each PI solution extracted from either MT-2 or MT-4 cells as described above was injected (25 μl) and analyzed using RP-HPLC/electrospray ionization (ESI)-MS. Drugs were separated on a VyDac C_{18} 5-μm-particle-size column (3.2 mm by 150 mm) using a gradient of solvent A (water–0.05% TFA–0.025% formic acid [FA]) and solvent B (acetonitrile–0.05% TFA–0.025% FA). The flow rate was set to 0.5 ml min^{-1}, and the column was equilibrated with 95% solvent A and 5% solvent B. Following each injection, solvent B was increased to 40% over a 35-min period (1% increase per min). At 35 min solvent B was increased to 95% in 2 min and then returned to starting conditions over the next 8 min. Each drug was detected by ESI-MS using an Agilent 1100 mass spectrometer in selective ion monitoring mode (SIM). The sodium adducts of each drug provided the most prominent peak and therefore were used for detection purposes although the parent ions provided the relative results. The reference masses for the sodium adduct-SIM ions used were 570.20, 599.20, and 598.20 for DRV, GRL007, and GRL008, respectively. The amount of drug obtained in the extracts was determined by comparison to standards of each purified drug in DMSO. Each compound was confirmed by both elution time from the column and molecular weight by mass spectrometry.

TABLE 1 Enzyme-inhibitory activity, antiviral activity, and cytotoxicity of GRL007 and GRL008

Inhibitor	K_i of PR^{WT} (pM)[b]	EC_{50} (μM) against HIV^{WT} in:[a]		CC_{50} (μM) in MT-4 cells
		MT-2 cells	MT-4 cells	
GRL007	12.7	>10	>1	>100
GRL008	8.9	0.093 ± 0.041	0.038 ± 0.015	>100
DRV	16	0.006 ± 0.001	0.002 ± 0.001	>100
TPV	8	ND[d]	0.128 ± 0.091	ND
SQV	40	ND	0.017 ± 0.012	11.3 ± 2.8[c]
APV	40	ND	0.032 ± 0.016	>100[c]

[a] EC_{50} (50% effective concentration) values are shown as mean values ± standard deviations from three independent experiments. HIV^{WT} strains used to infect MT-2 and MT-4 cells were HIV_{LAI} and HIV_{NL4-3}, respectively.
[b] The K_i values of PR^{WT} with TPV (32), SQV (33), and APV (33) were previously published.
[c] CC_{50} values were determined in MT-2 cells (14).
[d] ND, not determined.

Protein structure accession numbers. The final refined coordinates for the crystal structures of PR^{WT}-DRV, PR^{WT}-GRL007, and PR^{WT}-GRL008 were deposited in the Research Collaboratory for Structural Bioinformatics Protein Data Bank (RCSB PDB) under accession IDs 4HLA, 4I8W, and 4I8Z, respectively.

RESULTS

GRL007 and GRL008 are highly active *in vitro* against PR^{WT}. Evaluation of the *in vitro* enzyme-inhibitory activity of GRL007 and GRL008 revealed that both PIs highly effectively inhibit PR^{WT}. The enzyme inhibition constants (K_is) for GRL007 and GRL008 against PR^{WT} were 12.7 pM and 8.9 pM, respectively. As shown in Table 1, the K_i values of GRL007 and GRL008 were comparable to those of DRV and tipranavir (TPV) (32). Both GRL007 and GRL008 were >3-fold more active than saquinavir (SQV) (33) and amprenavir (APV) (33) (Table 1). These results suggest that GRL007 and GRL008 would be highly active PIs comparable to DRV and should be evaluated further for their binding profiles and antiviral potency although it is possible that various factors, such as cell penetration, intracellular sequestration, efflux, etc., of protease inhibitors can affect their ultimate antiviral potency to a great extent. Thus, we further investigated the binding profiles of GRL007 and GRL008 in the active site of PR^{WT} using X-ray crystallography.

Crystal structures of PR^{WT} in complex with DRV, GRL007, or GRL008. In order to understand the binding profiles of GRL007 and GRL008 with protease, PR^{WT} was cocrystallized with GRL007 or GRL008 or DRV, and the X-ray crystal structures were solved and analyzed. Cocrystals of PR^{WT} in complex with DRV

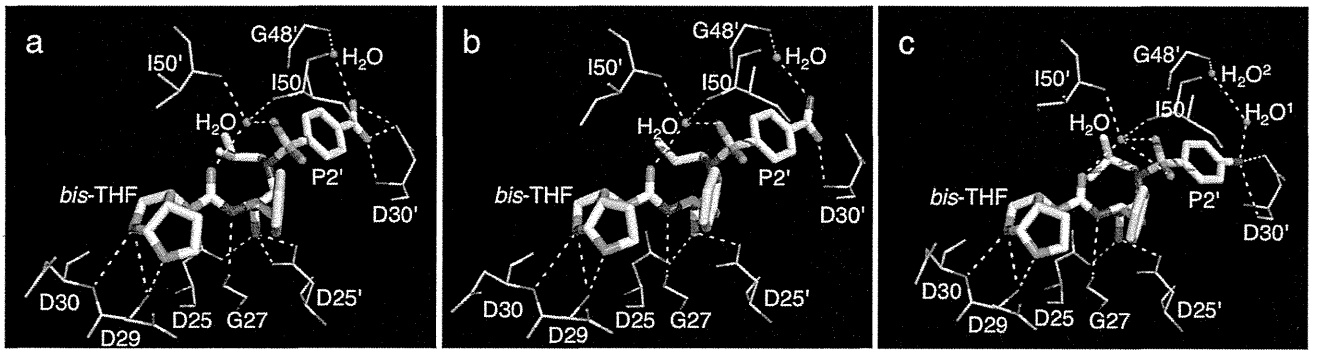

FIG 2 Polar contacts between PR^{WT} and inhibitors. Polar contacts of GRL007, GRL008, and DRV with PR^{WT} are shown in panels a, b, and c, respectively. The carbon atoms of PIs and PR^{WT} are shown as white and green sticks, respectively. Oxygen and nitrogen atoms are shown as red and blue sticks, respectively. Polar contacts in each panel are shown as yellow dashed lines. Conserved crystallographic waters are shown as red spheres. The P2 *bis*-THF moiety shows three conserved polar contacts with the backbone amide nitrogen atoms of Asp29 and Asp30. The P2′ moiety of each inhibitor shows at least one conserved polar contact, each with the backbone of Asp30′. In addition, GRL007 shows two direct polar contacts and DRV shows one direct polar contact with the δ-oxygen atom from the side chain of Asp30′. While two stable water molecules are seen bridging between the aniline moiety of DRV and Gly48′ of PR^{WT} (panel c), only one stable water is seen in the case of GRL007 (panel a) and GRL008 (panel b). This loss of a water molecule is compensated by the benzene carboxylic acid and benzene carboxamide groups. All polar contacts were calculated as the distances between the heavy atoms.

were obtained at pH 6.0 while cocrystals of PR^{WT} in complex with either GRL007 or GRL008 were obtained at pH 9.0. All cocrystals were obtained at room temperature, usually in 2 to 5 days using 1.6 M ammonium sulfate as a precipitant (ammonium sulfate grid screen from Hampton Research, Aliso Viejo, CA). The crystal structure of PR^{WT} in complex with GRL007, GRL008, or DRV was solved to a resolution of 1.95 Å, 1.75 Å, or 1.95 Å, respectively. All three structures were solved in the space group $P6_1$ with the following unit cell dimensions: a = 62, b = 62, c = 82, α = 90°, β = 90°, and γ = 90°. Each of the three crystal structures showed one protease dimer per asymmetric unit. Cocrystals of PR^{WT} in complex with GRL008 diffracted to 1.7 Å, while the cocrystals of PR^{WT} in complex with either GRL007 or DRV diffracted to 1.9 Å. All three structures showed >90% completeness, including the highest-resolution shells (see Table S1 in the supplemental material). The difference electron density maps indicated two binding orientations (separated by 180°) for each PI in the active site of PR^{WT}. As shown in Fig. S1, the average difference electron density maps for each PI (contoured between 2.0 and 2.5 σ) showed continuous density for one orientation (orientation 1) and semicontinuous density for the second orientation (orientation 2). In each case, the PI was fit in both orientations with an initial occupancy of 0.5 per orientation, and the final refined occupancies ranged between 0.48 and 0.52. In each case, the refined binding conformation of the PI with higher occupancy was used for further structural analysis. The quality of the stereochemistry was evaluated using Ramachandran plots. None of the three structures showed any residues in the disallowed region (see Table S2 in the supplemental material), indicating an overall good quality of the stereochemistry.

GRL007 and GRL008 show similar binding profiles in the active site of PR^{WT}. Analysis of the refined structures revealed that each PI is involved in multiple polar contacts with PR^{WT} (Fig. 2). The *bis*-THF moiety at P2 shows three strong polar contacts with the backbone amide nitrogen atoms of Asp29 (two contacts) and Asp30 (one contact) in all three structures. The average bond lengths for these polar contacts (between the *bis*-THF moiety and either D29 or D30) range between 2.8 Å and 3.4 Å, indicating that these interactions with protease backbone are strong. One polar contact with the backbone carbonyl oxygen atom of Gly27 (average bond length of 3.25 Å) was also observed in all three structures. The transition state-mimetic hydroxyl group of each PI shows at least one polar contact each with either δ-oxygen atom from the side chains of the catalytic Asp25 and Asp25′. As shown in Fig. 2, the P2′ moieties, benzene carboxylic acid (GRL007) and benzene carboxamide (GRL008), show one strong polar contact each with the backbone amide nitrogen atom of Asp30′, while the P2′ aniline (DRV) shows one polar contact with the backbone carbonyl oxygen atom of Asp30′. The P2′ benzene carboxylic acid (GRL007) and aniline (DRV) show additional contact(s) with the δ-oxygen atom of the side chain of Asp30′ (Fig. 2). One conserved water molecule bridging between each PI and the PR^{WT}-flap residues, Ile50 and Ile50′, was observed in all three structures.

GRL007 and GRL008 replaced one bridging water molecule in the S2′ binding pocket of PR^{WT}. The crystal structure of PR^{WT} in complex with DRV showed two water molecules (H_2O^1 and H_2O^2) bridging between the P2′ amine group from the aniline moiety of DRV and the backbone amide nitrogen atom of Gly48′ from the S2′ binding pocket of PR^{WT} (Fig. 2). The interatomic distances for these three polar contacts (from DRV to H_2O^1, H_2O^1 to H_2O^2, and H_2O^2 to Gly48′) were 2.4 Å, 3.9 Å, and 3.1 Å, respectively. This indicates that the polar contact between H_2O^1 and H_2O^2 was weakest among the three, suggesting that replacing one of these two water molecules with a modified P2′ moiety of DRV might enhance the binding in S2′ pocket of PR^{WT}. Crystal structures of PR^{WT} in complex with GRL007 or GRL008 showed one bridging water molecule between the backbone amide nitrogen atom of Gly48′ and their respective P2′ moieties. The interatomic distances for the two polar contacts (from GRL007 [P2′ benzene carboxylic acid moiety] to H_2O and from H_2O to Gly48′) were 3.2 Å and 2.9 Å, respectively. Similarly, the interatomic distances for the two polar contacts (from GRL008 [P2′ benzene carboxamide moiety] to H_2O and from H_2O to Gly48′) were 3.1 Å and 2.9 Å, respectively. Based on the distance cutoff, the bridging polar contacts made by the P2′ moieties of either GRL007 or GRL008 with Gly48′ were considered to be stronger than those of DRV. Thus, the P2′ benzene carboxylic acid and benzene carboxamide groups

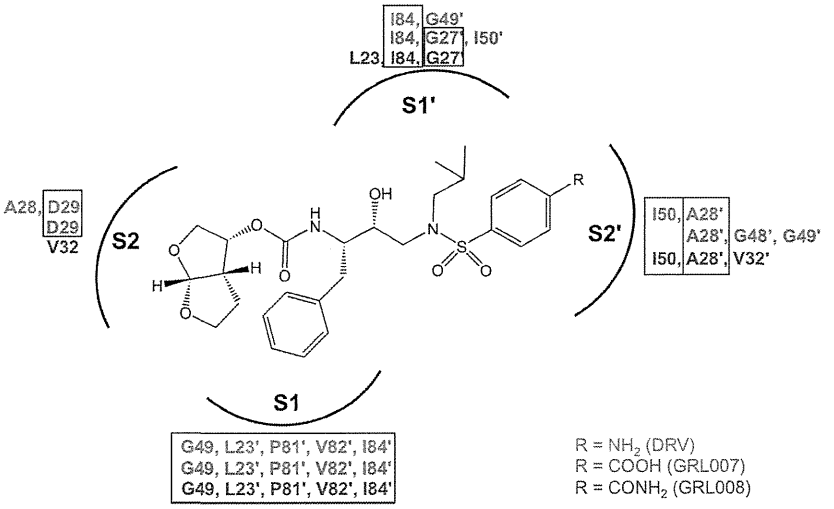

FIG 3 Distribution of hydrophobic contacts for DRV, GRL007, and GRL008. The amino acid residues from PR^{WT} that are involved in hydrophobic interactions with DRV, GRL007, or GRL008 are shown here in green, red, and blue, respectively. All three PIs show a conserved trend of contacts in the S1 binding pocket but variable contacts in the S1′ binding pocket due to altered binding orientations of the P1′ isopropyl group. The *bis*-THF moiety of each PI shows contacts with at least one residue in the S2 binding pocket. GRL007 and GRL008 show more contacts in the S1′ and S2′ pockets than DRV. Residues that show conserved contacts with two or all three PIs are boxed in black.

of GRL007 and GRL008, respectively, replaced one of the two bridging waters seen with DRV.

GRL007 and GRL008 show altered but persistent hydrophobic contacts compared to DRV. Hydrophobic contacts play a very important role in enhancing the binding affinity of PIs to the PR^{WT} in combination with polar contacts. The P1′ isopropyl group showed altered binding orientations among the three crystal structures (Fig. 2). These minor alterations of the P1′ isopropyl group in combination with a change in the P2′ moieties of each PI caused alterations in the overall pattern of hydrophobic contacts among the three PIs. As shown in Fig. 3, GRL007, GRL008, and DRV each showed hydrophobic interactions with 12, 12, and 11 residues, respectively, in the active site of PR^{WT}. While GRL007 and GRL008 each showed hydrophobic contacts with six residues in the S2/S1 binding pockets of PR^{WT}, DRV showed contacts with seven residues. Similarly, GRL007 and GRL008 each showed hydrophobic contacts with six residues in the S1′/S2′ binding pockets of PR^{WT}; DRV showed contacts with four residues. All three PIs showed conserved hydrophobic contacts with five residues in the S1 binding pocket. DRV showed equal distribution of average hydrophobic contacts per residue in both the S2/S1 and S1′/S2′ binding pockets of PR^{WT}, while both GRL007 and GRL008 showed relatively more average hydrophobic contacts per residue in the S1′/S2′ pockets of PR^{WT}. Residues G49, I84, L23′, A28′, P81′, V82′, and I84′ showed persistent hydrophobic contacts in all three structures. In addition, G27′ showed conserved hydrophobic contacts in crystal structures of PR^{WT} in complex with GRL007 and GRL008. Thus, the overall profiles of hydrophobic contacts for GRL007 and GRL008, in spite of small alterations, indicate strong binding comparable to or even better than that of DRV. These binding profiles thus support the picomolar enzyme-inhibitory activity of both GRL007 and GRL008.

GRL008 shows greater potency than GRL007 in cell-based antiviral assays. Guided by the favorable K_i values and binding profiles, we subsequently examined the antiviral activity of GRL007 and GRL008 in a cell-based assay. Antiviral assays using human MT-2 and MT-4 cells (Table 1) showed that GRL008 was highly active against HIV^{WT} with EC_{50}s of 0.093 and 0.038 μM (>100- and >25-fold more potent, respectively, than GRL007). GRL007 showed no antiviral activity at up to 10 and 1 μM concentrations in MT-2 and MT-4 cells, respectively. Although the antiviral potency of GRL008 against HIV^{WT} was within a 2.5-fold range of the potency of two other FDA-approved PIs, APV and SQV, it was >3-fold potent than TPV as tested in the assay using MT-4 cells. DRV was found to be the most potent among all the PIs tested in this assay using both MT-2 and MT-4 cells, with EC_{50}s of 0.006 and 0.002 μM, respectively. As shown in Table 1, both GRL007 and GRL008 had reasonably favorable cytotoxicity profiles, comparable to the cytotoxicity profile of DRV. The therapeutic window (the ratio of the 50% cytotoxic concentration [CC_{50}] to EC_{50}) of GRL008 was >2,600, suggesting that it could be a safe and active compound worth evaluating further. Thus, in spite of potent enzyme-inhibitory activity, favorable binding, and reasonable cytotoxicity profiles, it was concluded that GRL007 exhibits very poor antiviral activity in cell-based assays. Thus, we attempted to examine whether the cellular uptake of GRL007 might be a factor virtually nullifying its antiviral activity.

Significantly lower intracellular concentrations of GRL007 than GRL008 found in HPLC/MS-based cellular uptake assays. An HPLC/MS-based cellular uptake assay was used to examine the cellular uptake of GRL007 in human MT-2 and MT-4 cells. Dried solvent extracts of either MT-2 or MT-4 cells, preincubated with a 50 μM concentration of each PI, were dissolved in DMSO and analyzed using RP-HPLC/ESI-MS. The chromatograms (Fig. 4) revealed significantly higher intracellular concentrations of GRL008 and DRV than that of GRL007 in the cell extracts derived from human MT-2 and MT-4 cells prepared under identical conditions. The percent area under the curve (AUC) for each PI is illustrated in Fig. 5, where the AUC associated with DRV served as a reference (100% AUC). Indeed, both cell lines showed very low uptake for GRL007. While MT-2 cells showed greater uptake of DRV than that of GRL008, MT-4 cells showed greater uptake of

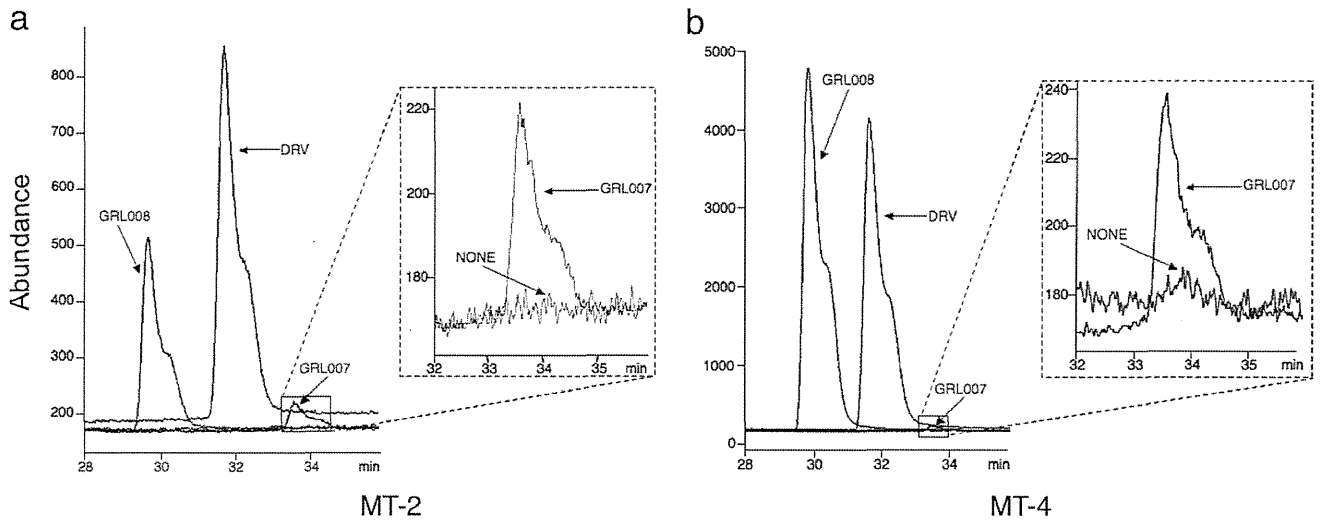

FIG 4 RP-HPLC/MS chromatograms of PIs. Overlays of chromatograms (GRL007, GRL008, and DRV) obtained from RP-HPLC/ESI-MS analysis of MT-2 and MT-4 cell extracts are shown, as indicated. Peak elution time (*x* axis) was plotted against the peak abundance on the *y* axis. Each chromatogram shows two prominent peaks (GRL008 and DRV) and a small peak (GRL007). An enlarged view of the small peak (GRL007) along with background is shown for clarity in insets. The smaller peak for GRL007 in either cell line indicates its poor cell penetration property compared to that of GRL008 or DRV.

GRL008 than that of DRV. It is of note that irrespective of intracellular concentrations of DRV, the potency of DRV was greater than that of GRL008. This could be due to intracellular nonspecific binding of GRL008, potentially owing to the relatively higher polar nature of its P2′ benzene carboxamide moiety (caused by the delocalization of a lone pair of electrons on the nitrogen atom) than the P2′ aniline moiety of DRV.

DISCUSSION

The present structure-function studies show that minor chemical modifications of PIs such as DRV might enhance the *in vitro* activity against PR^{WT} but compromise the antiviral potency of the modified compound either severely (as seen for GRL007) or moderately (as seen for GRL008). The P2′ benzene carboxylic acid and benzene carboxamide groups of GRL007 and GRL008, respectively, replaced one of the two bridging waters seen with DRV, while still retaining the polar contact with the backbone amide nitrogen atom of Asp30′ as well as with Gly48′ through one conserved bridging water molecule (Fig. 2). This bridging water molecule could be used as a molecular clue in future optimization of the benzene carboxylic acid and benzene carboxamide moieties to achieve a direct polar contact with Gly48′. The P2′ benzene carboxamide moiety of GRL008, due to delocalization of the lone pair of electrons on the nitrogen atom caused by the carbonyl oxygen atom, shows a strong direct polar contact between the carbonyl oxygen atom of the benzene carboxamide moiety and the backbone amide nitrogen atom of Asp30′ (Fig. 2). In the case of GRL007, equal polarity may be seen for both oxygen atoms of the carboxyl group from the P2′ benzene carboxylic acid moiety due to delocalization of electrons equally between the two oxygen atoms. Hence, strong direct polar contacts with the backbone (amide nitrogen atom) as well as the side chain (δ-oxygen atom) of Asp30′ were observed (Fig. 2). Thus, the crystal structures support the highly effective inhibition of PR^{WT} by GRL007 and GRL008.

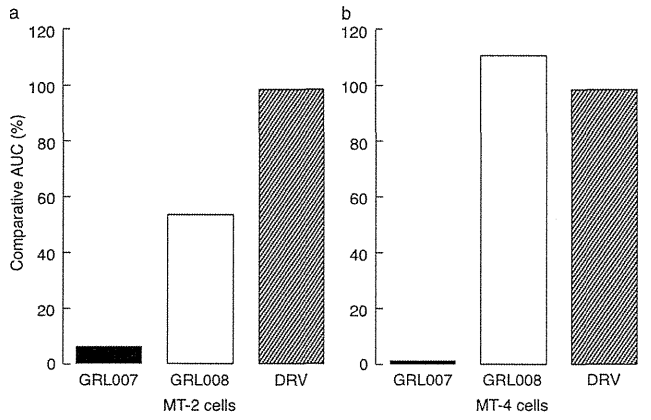

FIG 5 Percent areas under the curve determined for GRL007 and GRL008. Values for the percent area under the curve (AUC) of GRL007 and GRL008 determined using MT-2 and MT-4 cell extracts are shown, as indicated. Among the three inhibitors, GRL007 shows the lowest AUC, suggesting the poor cellular uptake of the inhibitor. DRV shows better uptake than GRL008 in MT-2 cell extracts, while the AUC for GRL008 in MT-4 cell extracts is relatively greater than that of DRV.

Intracellular concentrations of PIs have previously been described as a dynamic balance between influx, efflux, and sequestration (34). Since DRV serves as a transport substrate of P-glycoprotein (P-gp) (drug efflux transporter) (35), similar efflux profiles can be expected for GRL007 and GRL008 because P-gp has been shown to bind structurally diverse drugs (36). Assuming similar efflux profiles for GRL007 and GRL008, the sequestration and influx profiles of these PIs are of great interest. In the present study, HPLC/MS-based cellular uptake assays revealed significantly lower intracellular concentrations of GRL007 than of GRL008 and DRV. This suggests that the poor antiviral potency of GRL007 is unlikely due to the intracellular sequestration (ion trapping in acidic compartments or organelle trapping) but could be due to poor influx. Benzene carboxylic acid has been widely used either with minor modifications or as a component of small-

molecule drugs. For example, salicylic acid (2-hydroxybenzoic acid), the active metabolite of aspirin (acetyl salicylic acid), is a benzene carboxylic acid derivative. It has been shown that such benzene carboxylic acid derivatives are efficiently taken up by the cells with the help of transporters such as monocarboxylate transporter-1 (MCT1) (37). Similarly, benzene carboxylic acid has been used as a component of antidiabetics such as repaglinide (38) and VLA-4 (very late antigen 4) inhibitors (39) with good absorption profiles. Probenecid, an inhibitor of the renal organic anion transporter (drug influx transporter) (40) and a uricosuric drug that is often used to treat gout through peroral administration (41), coincidentally contains a benzene carboxylic acid moiety, the structure of the P2′ moiety of GRL007. Structural resemblance between probenecid and the P2′ moiety of GRL007 might make GRL007 an inhibitor rather than a substrate for a drug influx transporter. While both salicylic acid (contains benzene carboxylic acid) and salicylamide (42) (contains benzene carboxamide) have been clinically used as oral agents, the present structure-function data suggest that benzene carboxylic acid in combination with *bis*-THF might cause a significant decrease in cell penetration, resulting in poor antiviral properties (as seen for GRL007), but not the combination of benzene carboxamide and *bis*-THF, in line with the reasonably good antiviral potency of GRL008.

It has previously been shown that modification of polar groups (phosphonic acid) of an experimental PI, GS-8373 (molecular weight ([MW] of 672.68), as a diethyl ester derivative resulting in GS-8374 (MW of 728.79), significantly enhanced cell permeability and antiviral activity (43). Both GS-8373 and GS-8374 showed a >100-Da increase in their molecular masses compared to their parent compound, TMC-126 (MW of 562.67), deviating from Lipinski's rule of five (44). One can design similar prodrugs that are esters of GRL007 (MW of 576.66) to enhance its cell permeability, but GRL008 (MW of 575.67), with a minor modification, showed significantly enhanced cell permeability (Fig. 5) with a smaller increase (<30 Da) in molecular mass than that of the parent compound, DRV (MW of 547.24). Thus, further chemical modifications of GRL008, with favorable antiviral activity and cytotoxicity (Table 1), would be of interest. Moreover, the prodrugs of GRL007 may have compromised cytotoxicity, as seen for GS-8374 (43).

Based on our present structure-function studies, it is obvious that the examination of enzymatic activity of candidate compounds as PIs is not always suitable for evaluating their potential for ultimate clinical applications. As discussed above, various factors such as cell penetration (as in the case of GRL007), intracellular sequestration, and efflux can influence the outcome to a great extent in spite of a favorable enzyme-inhibitory profile. Cell-based antiviral assays are comparatively more crucial for evaluating their potential for further clinical applications. Moreover, the PIs which show favorable antiviral activity in cell-based assays never hold firm promises for further clinical applications. Even when certain PIs proved to be nontoxic and highly active against various HIV-1 strains, including existing multidrug-resistant HIV-1 strains, various challenges, including oral bioavailability and degradation due to the PIs' high susceptibility to drug-metabolizing enzymes such as cytochrome P450 3A4, may act as limiting factors. Compartmentalization of the PIs may also play a significant role in therapeutic concentrations in various cells and organs.

In conclusion, the P2′ benzene carboxylic acid in combination with P2 *bis*-THF can cause overall poor cell penetration, as seen in the case of GRL007, in spite of high enzyme-inhibitory activity. The P2′ benzene carboxamide (GRL008) or aniline (DRV) group is preferred in combination with the P2 *bis*-THF to achieve good cell penetration and therefore greater antiviral potency. It is warranted that GRL008 with desirable binding and inhibitory profiles against HIV^{WT} be further optimized to enhance its antiviral potency.

ACKNOWLEDGMENTS

This study was supported in part by the Intramural Research Program of Center for Cancer Research, National Cancer Institute, National Institutes of Health (H.M.), in part by a grant from a global education and research center aiming at the control of AIDS (Global Center of Excellence supported by Monbu-Kagakusho), Promotion of AIDS Research from the Ministry of Health, Welfare, and Labor of Japan, by a grant to the Cooperative Research Project on Clinical and Epidemiological Studies of Emerging and Re-emerging Infectious Diseases (Renkei Jigyo: number 78, Kumamoto University) of Monbu-Kagakusho (H.M.), and by a grant from the National Institutes of Health (GM53386 to A.K.G.). Use of the Advanced Photon Source was supported by the U.S. Department of Energy, Office of Science, Office of Basic Energy Sciences, under contract number DE-AC02-06CH11357 (Life Sciences Collaborative Access Team [LS-CAT]) and contract number W-31-109-Eng-38 (Southeast Regional Collaborative Access Team [SER-CAT]). Use of LS-CAT Sector 21 was supported by the Michigan Economic Development Corporation and the Michigan Technology Tri-Corridor for the support of this research program (grant 085P1000817). Supporting institutions for SER-CAT may be found at www.ser-cat.org/members.html.

We thank David W. Smith (LS-CAT) and beamline staff (SER-CAT) at the Advanced Photon Source for helping us with X-ray diffraction data collection. We thank the NIH AIDS Research and Reference Reagent program for APV, SQV, and TPV.

REFERENCES

1. Cohen MS, Chen YQ, McCauley M, Gamble T, Hosseinipour MC, Kumarasamy N, Hakim JG, Kumwenda J, Grinsztejn B, Pilotto JHS, Godbole SV, Mehendale S, Chariyalertsak S, Santos BR, Mayer KH, Hoffman IF, Eshleman SH, Piwowar-Manning E, Wang L, Makhema J, Mills LA, de Bruyn G, Sanne I, Eron J, Gallant J, Havlir D, Swindells S, Ribaudo H, Elharrar V, Burns D, Taha TE, Nielsen-Saines K, Celentano D, Essex M, Fleming TR. 2011. Prevention of HIV-1 infection with early antiretroviral therapy. N. Engl. J. Med. 365:493–505.
2. Lalezari JP, Eron JJ, Carlson M, Cohen C, DeJesus E, Arduino RC, Gallant JE, Volberding P, Murphy RL, Valentine F, Nelson EL, Sista PR, Dusek A, Kilby JM. 2003. A phase II clinical study of the long-term safety and antiviral activity of enfuvirtide-based antiretroviral therapy. AIDS 17:691–698.
3. Maeda K, Das D, Nakata H, Mitsuya H. 2012. CCR5 inhibitors: emergence, success, and challenges. Expert Opin. Emerg. Drugs 17:135–145.
4. Mitsuya H, Weinhold KJ, Furman PA, St Clair MH, Lehrman SN, Gallo RC, Bolognesi D, Barry DW, Broder S. 1985. 3′-Azido-3′-deoxythymidine (BW A509U): an antiviral agent that inhibits the infectivity and cytopathic effect of human T-lymphotropic virus type III/lymphadenopathy-associated virus in vitro. Proc. Natl. Acad. Sci. U. S. A. 82:7096–7100.
5. Steigbigel RT, Cooper DA, Kumar PN, Eron JE, Schechter M, Markowitz M, Loutfy MR, Lennox JL, Gatell JM, Rockstroh JK, Katlama C, Yeni P, Lazzarin A, Clotet B, Zhao J, Chen J, Ryan DM, Rhodes RR, Killar JA, Gilde LR, Strohmaier KM, Meibohm AR, Miller MD, Hazuda DJ, Nessly ML, DiNubile MJ, Isaacs RD, Nguyen B-Y, Teppler H. 2008. Raltegravir with optimized background therapy for resistant HIV-1 infection. N. Engl. J. Med. 359:339–354.
6. Ghosh AK, Dawson ZL, Mitsuya H. 2007. Darunavir, a conceptually new HIV-1 protease inhibitor for the treatment of drug-resistant HIV. Bioorg. Med. Chem. 15:7576–7580.
7. Kohl NE, Emini EA, Schleif WA, Davis LJ, Heimbach JC, Dixon RA, Scolnick EM, Sigal IS. 1988. Active human immunodeficiency virus pro-

tease is required for viral infectivity. Proc. Natl. Acad. Sci. U. S. A. 85:4686–4690.
8. Peng C, Ho BK, Chang TW, Chang NT. 1989. Role of human immunodeficiency virus type 1-specific protease in core protein maturation and viral infectivity. J. Virol. 63:2550–2556.
9. Meek TD, Dayton BD, Metcalf BW, Dreyer GB, Strickler JE, Gorniak JG, Rosenberg M, Moore ML, Magaard VW, Debouck C. 1989. Human immunodeficiency virus 1 protease expressed in *Escherichia coli* behaves as a dimeric aspartic protease. Proc. Natl. Acad. Sci. U. S. A. 86:1841–1845.
10. Graves MC, Lim JJ, Heimer EP, Kramer RA. 1988. An 11-kDa form of human immunodeficiency virus protease expressed in *Escherichia coli* is sufficient for enzymatic activity. Proc. Natl. Acad. Sci. U. S. A. 85:2449–2453.
11. Preston BD, Dougherty JP. 1996. Mechanisms of retroviral mutation. Trends Microbiol. 4:16–21.
12. Shafer RW, Rhee S-Y, Pillay D, Miller V, Sandstrom P, Schapiro JM, Kuritzkes DR, Bennett D. 2007. HIV-1 protease and reverse transcriptase mutations for drug resistance surveillance. AIDS 21:215–223.
13. Yedidi RS, Proteasa G, Martinez JL, Vickrey JF, Martin PD, Wawrzak Z, Liu Z, Kovari IA, Kovari LC. 2011. Contribution of the 80s loop of HIV-1 protease to the multidrug-resistance mechanism: crystallographic study of MDR769 HIV-1 protease variants. Acta Crystallogr. D Biol. Crystallogr. 67:524–532.
14. Koh Y, Nakata H, Maeda K, Ogata H, Bilcer G, Devasamudram T, Kincaid JF, Boross P, Wang Y-F, Tie Y, Volarath P, Gaddis L, Harrison RW, Weber IT, Ghosh AK, Mitsuya H. 2003. Novel bis-tetrahydrofuranylurethane-containing nonpeptidic protease inhibitor (PI) UIC-94017 (TMC114) with potent activity against multi-PI-resistant human immunodeficiency virus *in vitro*. Antimicrob. Agents Chemother. 47:3123–3129.
15. Koh Y, Matsumi S, Das D, Amano M, Davis DA, Li J, Leschenko S, Baldridge A, Shioda T, Yarchoan R, Ghosh AK, Mitsuya H. 2007. Potent inhibition of HIV-1 replication by novel non-peptidyl small molecule inhibitors of protease dimerization. J. Biol. Chem. 282:28709–28720.
16. McKeage K, Perry CM, Keam SJ. 2009. Darunavir: a review of its use in the management of HIV infection in adults. Drugs 69:477–503.
17. Mitsuya Y, Liu TF, RheeS-Y, Fessel WJ, Shafer RW. 2007. Prevalence of darunavir resistance-associated mutations: patterns of occurrence and association with past treatment. J. Infect. Dis. 196:1177–1179.
18. Koh Y, Amano M, Towata T, Danish M, Leshchenko-Yashchuk S, Das D, Nakayama M, Tojo Y, Ghosh AK, Mitsuya H. 2010. In vitro selection of highly darunavir-resistant and replication-competent HIV-1 variants by using a mixture of clinical HIV-1 isolates resistant to multiple conventional protease inhibitors. J. Virol. 84:11961–11969.
19. Ghosh AK, Leshchenko S, Noetzel M. 2004. Stereoselective photochemical 1,3-dioxolane addition to 5-alkoxymethyl-2(5H)-furanone: synthesis of bis-tetrahydrofuranyl ligand for HIV protease inhibitor UIC-94017 (TMC-114). J. Org. Chem. 69:7822–7829.
20. Cheng Y-SE, McGowan MH, Kettner CA, Schloss JV, Erickson-Viitanen S, Yin FH. 1990. High-level synthesis of recombinant HIV-1 protease and the recovery of active enzyme from inclusion bodies. Gene 87:243–248.
21. Otwinowski Z, Minor W. 1997. Processing of x-ray diffraction data collected in oscillation mode. Methods Enzymol. 276:307–326.
22. Leslie AG. 2006. The integration of macromolecular diffraction data. Acta Crystallogr. D Biol. Crystallogr. 62:48–57.
23. Evans P. 2006. Scaling and assessment of data quality. Acta Crystallogr. D Biol. Crystallogr. 62:72–82.
24. Collaborative Computational Project, Number 4. 1994. The CCP4 suite: programs for protein crystallography. Acta Crystallogr. D Biol. Crystallogr. 50:760–763.
25. Vagin A, Teplyakov A. 1997. MOLREP: an automated program for molecular replacement. J. Appl. Crystallogr. 30:1022–1025.
26. Murshudov GN, Vagin AA, Dodson EJ. 1997. Refinement of macromolecular structures by the maximum-likelihood method. Acta Crystallogr. D Biol. Crystallogr. 53:240–255.
27. Lamzin VS, Wilson KS. 1993. Automated refinement of protein models. Acta Crystallogr. D Biol. Crystallogr. 49:129–147.
28. Zwart PH, Langer GG, Lamzin VS. 2004. Modelling bound ligands in protein crystal structures. Acta Crystallogr. D Biol. Crystallogr. 60:2230–2239.
29. Schuttelkopf AW, van Aalten DMF. 2004. PRODRG: a tool for high-throughput crystallography of protein-ligand complexes. Acta Crystallogr. D Biol. Crystallogr. 60:1355–1363.
30. Adams PD, Afonine PV, Bunkoczi G, Chen VB, Davis IW, Echols N, Headd JJ, Hung L-W, Kapral GJ, Grosse-Kunstleve RW, McCoy AJ, Moriarty NW, Oeffner R, Read RJ, Richardson DC, Richardson JS, Terwilliger TC, Zwart PH. 2010. PHENIX: a comprehensive Python-based system for macromolecular structure solution. Acta Crystallogr. D Biol. Crystallogr. 66:213–221.
31. Davis DA, Singer KE, Reynolds IP, Haque M, Yarchoan R. 2007. Hypoxia enhances the phosphorylation and cytotoxicity of ganciclovir and zidovudine in Kaposi's sarcoma-associated herpesvirus–infected cells. Cancer Res. 67:7003–7010.
32. Turner SR, Strohbach JW, Tommasi RA, Aristoff PA, Johnson PD, Skulnick HI, Dolak LA, Seest EP, Tomich PK, Bohanon MJ, Horng M-M, Lynn JC, Chong K-T, Hinshaw RR, Watenpaugh KD, Janakiraman MN, Thaisrivongs S. 1998. Tipranavir (PNU-140690): a potent, orally bioavailable nonpeptidic HIV protease inhibitor of the 5,6-dihydro-4-hydroxy-2-pyrone sulfonamide class. J. Med. Chem. 41:3467–3476.
33. Spaltenstein A, Almond MR, Bock WJ, Cleary DG, Furfine ES, Hazen RJ, Kazmierski WM, Salituro FG, Tung RD, Wright LL. 2000. Novel inhibitors of HIV protease: design, synthesis and biological evaluation of picomolar inhibitors containing cyclic P1/P2 scaffolds. Bioorg. Med. Chem. Lett. 10:1159–1162.
34. Hoggard PG, Owen A. 2003. The mechanisms that control intracellular penetration of the HIV protease inhibitors. J. Antimicrob. Chemother. 51:493–496.
35. Fujimoto H, Higuchi M, Watanabe H, Koh Y, Ghosh AK, Mitsuya H, Tanoue N, Hamada A, Saito H. 2009. P-glycoprotein mediates efflux transport of darunavir in human intestinal Caco-2 and ABCB1 gene-transfected renal LLC-PK1 cell lines. Biol. Pharm. Bull. 32:1588–1593.
36. Zhou SF. 2008. Structure, function and regulation of P-glycoprotein and its clinical relevance in drug disposition. Xenobiotica 38:802–832.
37. Choi J-S, Jin MJ, Han H-K. 2005. Role of monocarboxylic acid transporters in the cellular uptake of NSAIDs. J. Pharm. Pharmacol. 57:1185–1189.
38. Balfour JA, Faulds D. 1998. Repaglinide. Drugs Aging 13:173–180.
39. Chiba J, Iimura S, Yoneda Y, Watanabe T, Muro F, Tsubokawa M, Iigou Y, Satoh A, Takayama G, Yokoyama M, Takashi T, Nakayama A, Machinaga N. 2007. Synthesis and biological evaluation of benzoic acid derivatives as potent, orally active VLA-4 antagonists. Bioorg. Med. Chem. 15:1679–1693.
40. Srimaroeng C, Perry JL, Pritchard JB. 2008. Physiology, structure, and regulation of the cloned organic anion transporters. Xenobiotica 38:889–935.
41. Pascale LR, Dubin A, Hoffman WS. 1952. Therapeutic value of probenecid (Benemid) in gout. JAMA 149:1188–1194.
42. Litter M, Moreno AR, Donin L. 1951. Salicylamide: pharmacology, fate and clinical use. J. Pharmacol. Exp. Ther. 101:119–124.
43. Callebaut C, Stray K, Tsai L, Williams M, Yang Z-Y, Cannizzaro C, Leavitt SA, Liu X, Wang K, Murray BP, Mulato A, Hatada M, Priskich T, Parkin N, Swaminathan S, Lee W, HeG-X, Xu L, Cihlar T. 2011. *In vitro* characterization of GS-8374, a novel phosphonate-containing inhibitor of HIV-1 protease with a favorable resistance profile. Antimicrob. Agents Chemother. 55:1366–1376.
44. Lipinski CA, Lombardo F, Dominy BW, Feeney PJ. 2001. Experimental and computational approaches to estimate solubility and permeability in drug discovery and development settings. Adv. Drug Deliv Rev. 46:3–26.

Journal of Medicinal Chemistry

Article

pubs.acs.org/jmc

Highly Potent HIV-1 Protease Inhibitors with Novel Tricyclic P2 Ligands: Design, Synthesis, and Protein–Ligand X-ray Studies

Arun K. Ghosh,*[,†] Garth L. Parham,[†] Cuthbert D. Martyr,[†] Prasanth R. Nyalapatla,[†] Heather L. Osswald,[†] Johnson Agniswamy,[‡] Yuan-Fang Wang,[‡] Masayuki Amano,[§] Irene T. Weber,[‡] and Hiroaki Mitsuya[§,∥]

[†]Department of Chemistry and Department of Medicinal Chemistry, Purdue University, West Lafayette, Indiana 47907, United States

[‡]Department of Biology, Molecular Basis of Disease, Georgia State University, Atlanta, Georgia 30303, United States

[§]Departments of Hematology and Infectious Diseases, Kumamoto University Graduate School of Medical and Pharmaceutical Sciences, Kumamoto 860-8556, Japan

[∥]Experimental Retrovirology Section, HIV and AIDS Malignancy Branch, National Cancer Institute, National Institutes of Health, Bethesda, Maryland 20892, United States

Supporting Information

ABSTRACT: The design, synthesis, and biological evaluation of a series of HIV-1 protease inhibitors incorporating stereochemically defined fused tricyclic P2 ligands are described. Various substituent effects were investigated to maximize the ligand-binding site interactions in the protease active site. Inhibitors **16a** and **16f** showed excellent enzyme inhibitory and antiviral activity, although the incorporation of sulfone functionality resulted in a decrease in potency. Both inhibitors **16a** and **16f** maintained activity against a panel of multidrug resistant HIV-1 variants. A high-resolution X-ray crystal structure of **16a**-bound HIV-1 protease revealed important molecular insights into the ligand-binding site interactions, which may account for the inhibitor's potent antiviral activity and excellent resistance profiles.

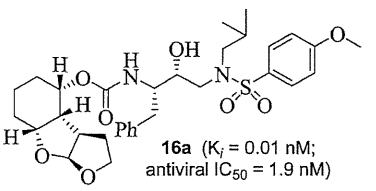

INTRODUCTION

HIV-1 protease inhibitors (PIs) are critical components of current antiretroviral therapies. However, the rapid emergence of drug-resistance severely compromises the clinical benefits of PIs.[1−3] In our continuing efforts to address issues of drug resistance, our inhibitor design strategy focuses on maximizing active-site interactions with the protease, particularly by promoting extensive hydrogen-bonding interactions with the backbone atoms throughout the active site.[4−6] Recently, our structure-based design targeting the protein backbone led to the discovery of exceedingly potent HIV-1 PI **1** (K_i = 5.9 pM, IC_{50} = 1.8 nM, Figure 1).[7,8] This inhibitor has shown a marked potency against a range of multidrug-resistant HIV-1 variants.[9] We determined that the syn-anti-syn-fused tricyclic ether (P2 ligand) in **1** is responsible for its enhanced broad-range potency compared to the related FDA approved inhibitor darunavir (DRV) (**2**).[4,10]

Our X-ray structural studies of **1**-bound HIV-1 protease revealed the formation of an extensive hydrogen-bonding network between the inhibitor and the active site.[7,8] Particularly, the P2 ligand is involved in strong hydrogen-bonding interactions with the backbone amides of conserved residues Asp 29 and Asp 30 in the S2 subsite. The tricyclic P2 ligand also appeared to fit nicely in the hydrophobic pocket formed by the surrounding side chains of the Ile47, Val32, Ile84, Leu76, and Ile50′ residues. This molecular insight has now led us to investigate a range of P2 ligands designed on the basis of the tricyclic platform in inhibitor **1**. In particular, we have been interested in investigating the syn-anti-syn tricyclic

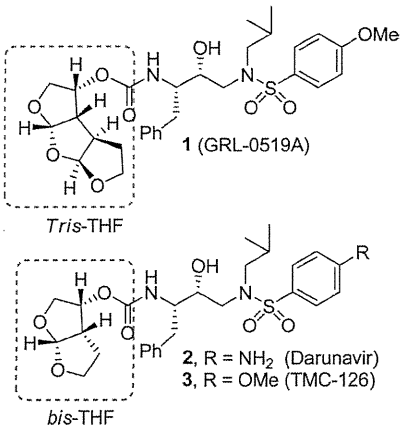

Figure 1. Structures of protease inhibitors **1**–**3**.

structural motif with functionalities that can interact with the conserved backbone and residues in the S2 subsite. We also planned to develop efficient methods for synthesizing these ligands rapidly using cycloaddition-based strategies. Herein, we report the design, synthesis, and biological evaluation of a series of novel HIV-1 PIs incorporating syn-anti-syn-fused tricyclic P2 ligands. Two of these inhibitors exhibited very potent antiviral activity against a panel of multidrug-resistant HIV-1 variants. A protein–ligand X-ray crystal structure of one of these inhibitors

Received: April 18, 2013
Published: August 15, 2013

provided important molecular insights into the ligand-binding site interactions.

CHEMISTRY

For the rapid synthesis of tricyclic P2 ligands, we planned to explore the feasibility of $Mn(OAc)_3$-based annulation of readily available 1,3-diketone derivatives and cyclic enol ethers such as dihydrofuran and dihydropyran. Similar annulation reactions have been shown to provide good yields of bicyclic derivatives efficiently.[11] The synthesis of our substituted fused tricyclic P2 ligands is shown in Scheme 1. Reactions of 1,3-diketones **4a,b**

Scheme 1. Synthesis of Tricyclic Ligands

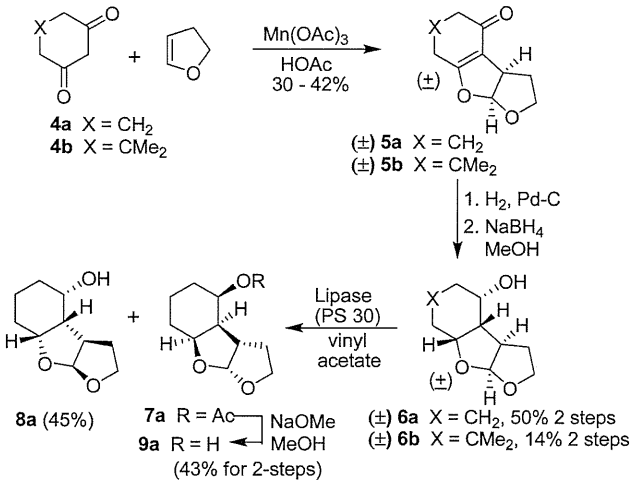

with dihydrofuran in the presence of $Mn(OAc)_3 \cdot 2H_2O$ in glacial acetic acid at 60 °C furnished the corresponding tricyclic derivatives **5a** (30% yield) and **5b** (42% yield). Enone **5a** was exposed to hydrogenation over 10% Pd–C in MeOH at 65 psi hydrogen pressure to give the corresponding ketone. The reduction of the resulting ketone with $NaBH_4$ in MeOH provided racemic endo alcohol **6a** in 50% yield in two steps. The syn-anti-syn relative ring stereochemistry of **6a** was supported by ^1H NMR NOESY experiments and was further confirmed by the X-ray structure of corresponding *p*-nitrobenzoate derivative **12** (Scheme 2).[12] The observed selectivity of the hydrogenation of **5a** presumably resulted from the directing effect by the terminal THF ring oxygen.[13] Further investigation is ongoing to determine the origin of the syn-anti-syn relative ring stereochemistry, and the details will be reported in due course. Hydrogenation of **5b** proceeded sluggishly to provide the corresponding ketone (17% yield). Subsequent $NaBH_4$ reduction (81% yield) afforded racemic alcohol **6b**.

Racemic alcohol **6a** was subjected to enzymatic resolution utilizing lipase PS-30 in vinyl acetate at 23 °C for 18 h.[14,15] The protocol provided optically active acetate derivative **7a** (45% yield) and alcohol **8a** (45% yield). Acetate **7a** was converted to the alcohol **9a** in 89% yield by transesterificaton using NaOMe in MeOH. Alcohol **8a** was converted to the corresponding Mosher ester, and ^{19}F NMR analysis revealed its optical purity to be 98% ee.[16] The absolute stereochemistry of alcohol **8a** was predicted on the basis of the Kazlauskas model as well as the optical resolution of structurally related bis-THF alcohols.[17] Ultimately, it was confirmed through X-ray analysis of the related oxygen-containing tricyclic derivative (Scheme 4). After

Scheme 2. Synthesis of Benzoate Ester 12 and Its Structure in an ORTEP Diagram

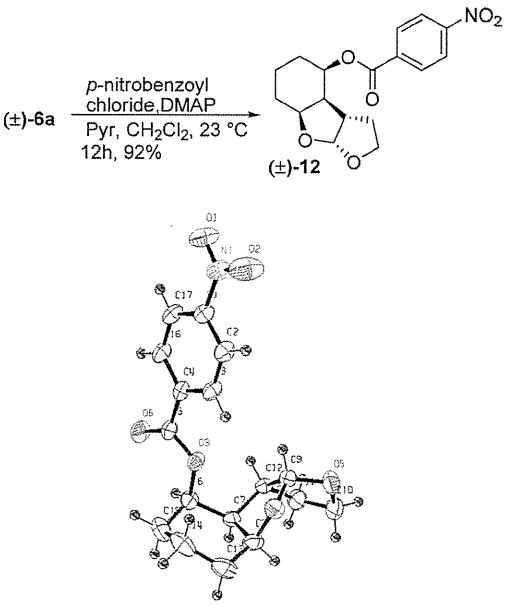

several unsuccessful attempts at resolving racemic alcohol **6b**, we decided to move forward with this ligand as a racemate.

We were also interested in evaluating the importance and effect of replacing the terminal furan in **8a** with a pyran ring. To this end, known diazo compound **11a**[18] was reacted with rhodium diacetate in 2,3-dihydro-4*H*-pyran to obtain intermediate **5c** in 77% yield, as shown in Scheme 3. In an effort to

Scheme 3. Synthesis of Heteroatom-Substituted Tricyclic P2 Ligands

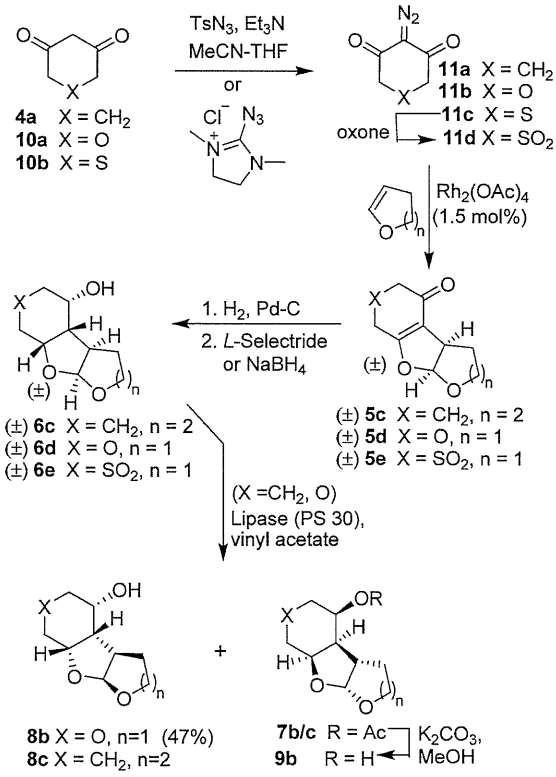

dx.doi.org/10.1021/jm400768f | J. Med. Chem. 2013, 56, 6792–6802

promote further polar interaction in the active site, we planned to incorporate a heteroatom within the cyclohexyl ring of the tricyclic ligand. Corresponding oxygen- and sulfur-containing 1,3-diketones **10a** and **10b** were synthesized on the basis of literature procedures.[19,20] However, the $Mn(OAc)_3$-based annulation of diketones **10a** and **10b** did not provide the desired enone. We then devised an alternate strategy. The synthesis of heteroatom-substituted tricyclic ligands is shown in Scheme 3. Diketone **10a** was converted to diazo derivative **11b** by treating the diketone with tosyl azide in the presence of Et_3N. This diazo transfer reaction also proceeded well for **11c** (68% yield) using procedures developed by Kitamura and co-workers.[21] Sulfide **11c** was conveniently oxidized to sulfone **11d** in 82% yield using oxone.[22,23] Diazo compounds **11b** and **11d** were subjected to rhodium-catalyzed carbenoid cyclo-addition with dihydrofuran using $Rh(OAc)_2$ (1.5 mol %) to afford fused heterocyclic compounds **5d** and **5e** in 67% and 48% yields, respectively.[24,25] The catalytic hydrogenation of enones **5d** and **5e** using 10% Pd–C in MeOH at 1 atm furnished the corresponding syn-anti-syn ketone. The reduction of the resulting ketones with L-selectride yielded racemic alcohols **6d** and **6e** in 23% and 28% yields over 2 steps, respectively. Enzymatic resolution of racemic alcohol **6d** provided optically pure alcohol **8b** in 47% yield and acetate **7b** in 48% yield.[14,15] Saponification of **7b** provided alcohol **9b** in 71% yield. Similarly, racemic alcohol **6c** was converted to optically active alcohols **8c** and acetate **7c**. After several unsuccessful attempts at enzymatic resolution, alcohol **6e** (X = SO_2) was carried through as a racemic mixture. The syn-anti-syn relative stereochemistry of **9b** was supported by ^1H NMR NOESY experiments. Ultimately, our determination of the X-ray structure of *p*-bromobenzoate **13**[12] confirmed the syn-anti-syn relative stereochemistry, as shown in Scheme 4.

The preparation of various *para*-nitrophenyl carbonates **14a–c** and **14e–h** is shown in Scheme 5. Various ligand alcohols were reacted with *para*-nitrophenyl chloroformate and pyridine in CH_2Cl_2 to provide mixed carbonates **14a–c** and

Scheme 4. ORTEP Diagram of syn-anti-syn Compound 13

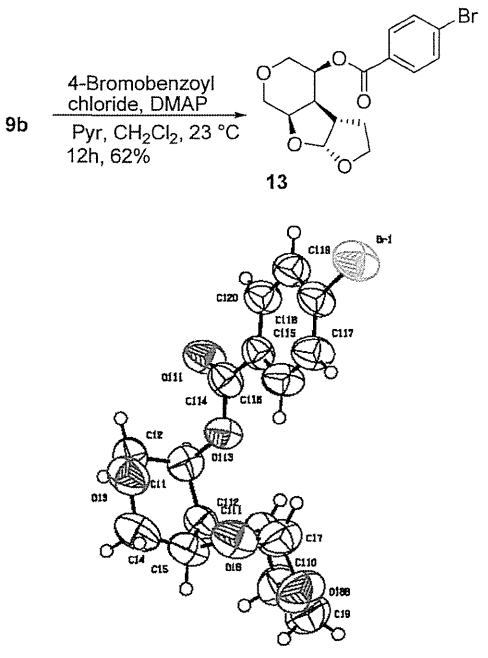

Scheme 5. Synthesis of Inhibitors 16a–i

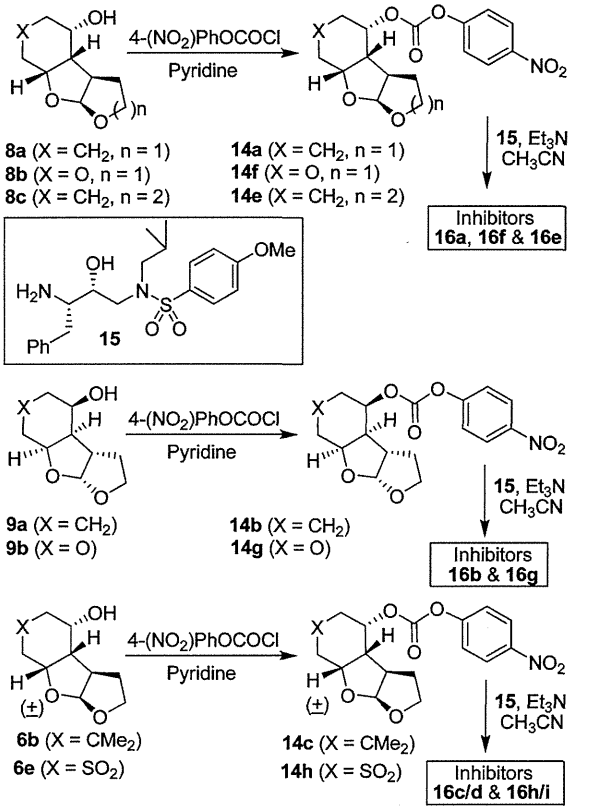

14e–h in good to excellent yields (70–97% yields).[26] The syntheses of HIV-1 protease inhibitors **16a,b** and **16e–g** were carried out by treatment of optically active amine **15** in the presence of Et_3N with carbonates obtained from optically active alcohols **8a–c** and **9a,b**. These inhibitors were obtained in 50–82% yields. For the syntheses of inhibitors **16c,d,h,i**, the corresponding carbonates derived from racemic alcohols **6b** and **6e** were reacted with optically active amine **15** in the presence of Et_3N to provide the corresponding mixture of diastereomeric inhibitors. Separation of these inhibitors by HPLC using a reverse-phase analytical column provided pure inhibitors **16c,d,h,i.** Stereochemical assignment of the respective inhibitors with diastereomeric P2 ligands was made on the basis of the comparison of the HPLC retension time of the diastereomeric inhibitors as well as the comparison of the ^1H NMR data of inhibitors **16a,b** and **16e–g** synthesized using optically pure ligands.

RESULTS AND DISCUSSION

Inhibitors **16a–i** were initially evaluated in enzyme-inhibitory assays using the protocol reported by Toth and Marshall.[27] On the basis of the exhibited enzyme-inhibitory potency, selected inhibitors were further evaluated in antiviral assays. The results are shown in Table 1. Our depicted synthesis route allowed us to prepare both enantiomers of the tricyclic ligands. We have prepared and evaluated the effect of enantiomeric pure ligands with a syn-anti-syn ring stereochemistry. 4(*S*)-Cyclohexyl ligand-derived inhibitor **16a** exhibited very impressive enzyme and antiviral potency (K_i = 10 pM, antiviral IC_{50} = 1.9 nM) over inhibitor **16b** (K_i = 0.45 nM, antiviral IC_{50} = 240 nM), which has a 4(*R*)-configuration. This result is consistent with our previous finding with DRV and tricyclic P2 ligand in